chemosensors

MDPI

Review

Phthalocyanine and Porphyrin Derivatives and Their Hybrid Materials in Optical Sensors Based on the Phenomenon of Surface Plasmon Resonance

Tamara Basova

Nikolaev Institute of Inorganic Chemistry SB RAS, 630090 Novosibirsk, Russia; basova@niic.nsc.ru

Abstract: In this review, the state of research over the past fifteen years in the field of the applications of metal phthalocyanines and porphyrin derivatives as well as their hybrid materials with carbon nanotubes, metal oxides, and polymers in optical sensors based on the phenomenon of surface plasmon resonance (SPR) is analyzed. The first chapter of the review presents an analysis of works on the use of porphyrins and phthalocyanines in classical SPR sensors for the detection of gases and volatile organic vapors, as well as their improved modifications, such as total internal reflection ellipsometry (TIRE) and magneto-optical SPR (MOSPR) methods, while the second chapter is devoted to their application for the detection of various analytes in solutions. The third chapter of the review summarizes publications describing recent advances in the use of porous materials based on hybrids of carbon nanotubes and oxides with metal phthalocyanines. The fourth chapter describes two-dimensional metal-organic frameworks (MOFs) based on metal porphyrin derivatives as SPR sensitizers.

Keywords: phthalocyanines; porphyrins; surface plasmon resonance; optical sensors; carbon nanotubes; hybrid materials; metal-organic frameworks

Citation: Basova, T. Phthalocyanine and Porphyrin Derivatives and Their Hybrid Materials in Optical Sensors Based on the Phenomenon of Surface Plasmon Resonance. *Chemosensors* **2024**, *12*, 56. https://doi.org/10.3390/chemosensors12040056

Academic Editor: Marco Pisco

Received: 4 March 2024
Revised: 27 March 2024
Accepted: 5 April 2024
Published: 6 April 2024

1. Introduction

Due to their unique electronic structure and properties, metal phthalocyanines (MPc) and porphyrins are widely utilized in various types of chemical sensors, including resistive, solid-state ionic, and capacitance sensors, sensors based on field-effect transistors (FET), as well as optical, quartz crystal microbalance (QCM), and surface acoustic-wave (SAW) sensing devices [1]. The ability to widely vary the structure of these molecules both by introducing different central metals and by varying axial or peripheral substituents in the macroring allows researchers to obtain sensors for the determination of analytes of various natures, from simple gases to complex biological molecules. The introduction of various functional groups into substituents makes these compounds reactive, which allows them to be used as building blocks for the production of metal-organic frameworks [2,3], hybrid and composite materials with polymers [4], nanoparticles [5], and nanocarbon materials [6].

The literature abounds with works on the study of the possibility of using phthalocyanines and porphyrins in the form of solutions and thin films in various types of chemical sensors, among them are review articles. Several reviews were published on the application of phthalocyanines over the last 15 years. For example, in 2009, Öztürk et al. [7] published a brief review that included 40 references devoted to the methods of preparation of phthalocyanine sensing films and their sensing mechanisms with several analytes. In 2013, Bouvet et al. [8] published a mini-review that included 56 references in which they demonstrated the chemical variability of phthalocyanines for the preparation of their hybrids with polymers and carbon-based materials and showed their application as sensing layers of electrochemical and conductometric sensors. Information about the modification of electrodes in electrochemical sensors with phthalocyanine derivatives was summarized in

the review by Demir and co-authors [9]. The resistive sensors based on porphyrins, phthalocyanines, and their hybrid materials were also described in several recent reviews [10–12]. Paolesse and co-authors [13] devoted their review to the application of porphyrinoids in chemical sensors based on various principles of transduction.

The role of phthalocyanines and porphyrins as active layers of optical sensors is also very important. Optical sensors use various spectroscopic measurements, including fluorescence, optical absorption, Raman scattering, and surface plasmon resonance (SPR). While review articles on fluorescent and colorimetric sensors based on phthalocyanines and porphyrins have been written by researchers in recent years, systematic reviews on their use in sensors based on SPR phenomena are practically absent in the literature. At the same time, SPR sensors using these derivatives as active layers are utilized for the detection of reducing and oxidizing gases, volatile organic compounds (VOCs), pesticides, biological molecules, etc. (Figure 1). For example, Celiesiute et al. [14] summarized the data on various electrochromic sensors based on polymers, metal oxides, and coordination compounds. Among coordination compounds, they gave several examples of porphyrins and phthalocyanines, but their number was not numerous (12 refs., the last one was published in 2013). Several examples of phthalocyanine-based optical sensors were described in the review by Gounden and co-authors [15]. Francis et al. [16] carried out a detailed analysis of the literature devoted to porphyrin-based colorimetric and fluorescence sensors. Liu et al. summarized the data on the study of porphyrin/phthalocyanine-based 2D covalent organic frameworks as active layers of colorimetric sensors in their recent review [17]. At the same time, the data on phthalocyanine-based SPR sensors were summarized only in a book chapter in 2017 [1], but all cited references were published before 2010.

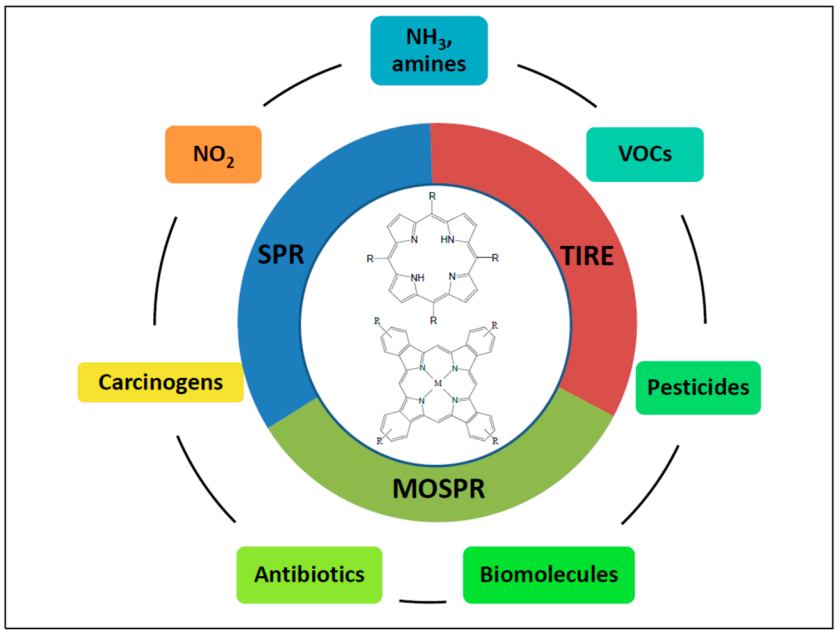

Figure 1. Scheme showing the use of optical sensors based on the phenomenon of plasmon resonance, using metal phthalocyanines and porphyrin derivatives as active layers.

In this review, the state of the research over the past fifteen years in the field of the applications of metal phthalocyanines and porphyrin derivatives as well as their hybrid materials with carbon nanotubes, metal oxides, and polymers in optical sensors based on the phenomenon of surface plasmon resonance is analyzed (Figure 1).

The first part of the review summarizes the data on classical SPR sensors for detecting gases and volatile organic vapors and their improved modifications, such as total internal reflection ellipsometry (TIRE) and magneto-optical SPR (MOSPR) methods. The second part is devoted to the application of phthalocyanines and porphyrins in sensors for the

detection of various analytes in solutions. The third chapter of the review presents an analysis of articles describing the latest advances in the use of porous materials based on hybrids of carbon nanotubes with metal phthalocyanines, while two-dimensional metal-organic frameworks (MOFs) based on metal porphyrin derivatives as SPR sensitizers are described in the fourth chapter.

2. Phthalocyanine- and Porphyrin-Based Sensors for the Detection of Gases and Volatile Organic Vapors

One of the important optical methods in which metal phthalocyanine films are used as sensing layers is the method based on the phenomenon of surface plasmon resonance. SPR is an extremely important method for studying interfacial binding processes. This method is utilized both for the detection of various gases and VOC vapors [18] and for the determination of biological and hazardous substances in solutions [19]. The classical SPR technique [15,20] and two improved modifications of this method are most often found in the literature. The last two modifications are the method of magneto-optical SPR (MOSPR) [21] and total internal reflection ellipsometry (TIRE) [22,23]. Examples of the use of these methods in which films of phthalocyanines and porphyrins, as well as their hybrid materials, play the role of sensing layers for the determination of gases and volatile organic vapors will be discussed in separate chapters below.

2.1. SPR Sensors

Surface plasmons are waves of variable electric charge density that can arise and propagate in the electron plasma of a metal along its surface or along a thin metal film. The resonant excitation of such oscillations by an electromagnetic wave in a thin layer of conductive material placed between two media with different refractive indices is called SPR [24]. SPR is a phenomenon of violation of the condition of total internal reflection in which a significant part of the energy of the light incident on the surface of the metal film is converted into the energy of plasmons, as a result of which the intensity of the light reflected from the surface of the metal film drops sharply. SPR is observed under the condition of total internal reflection and is characterized by a certain value of the refractive index of the substance above the metal surface and the angle of reflection in the minimum of the SPR spectrum. At a constant wavelength of the light source, the angle causing the SPR depends on the refractive index (n) of the material near the surface of a metal film (typically Au, Ag, Cu, or other plasmonic metals). As a result, any small change in n in the border region leads to a change in the SPR conditions. Detection is accomplished by measuring the changes in the reflected light obtained by a detector. This makes it possible to detect the analyzed substances on the surface. The principles of the SPR method used for sensing applications are described in a number of previous papers and book chapters [25,26]. Measurements are usually carried out in the Kretschmann configuration (Figure 2) [27]. The excitation of surface plasmons is achieved by focusing a p-polarized laser beam (λ = 633 nm) onto a prism/sample system, and the SPR is observed as a minimum of reflection when the angle of incidence of light changes, and the wavelength of light remains constant. SPR excitation can also be achieved by using an optical waveguide (OWG) instead of a prism, which is also known as waveguide-coupled SPR spectroscopy [28,29]. The values of refractive index (n), absorption coefficient (k), and film thickness (d) are determined by processing experimental data using the least squares minimization method of the modified Fresnel equation [30,31].

To prepare active layers for SPR sensors, thin films of porphyrins and phthalocyanines of various metals are deposited on a substrate covered with gold or silver. The properties of phthalocyanines and porphyrins, including their solubility and sensitivity to various assays, can be widely varied, both by changing a central metal and by introducing various substituents into the aromatic ring. The method of film deposition is chosen depending on the properties of the compounds. Films of porphyrins and phthalocyanines soluble in organic solvents are deposited by spin coating [1], Langmuir–Blodgett (LB), and Langmuir–

Schaefer (LS) [32–34] methods, while compounds that are volatile in a vacuum are deposited by vacuum deposition methods, namely physical vapor deposition (PVD) or organic molecular beam deposition (OMBD) [35,36].

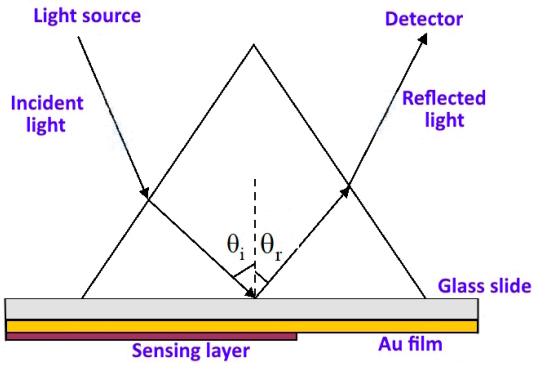

Figure 2. Kretschmann configuration used for SPR sensing.

Below, it will be considered how the molecular structure of phthalocyanines and porphyrins affects their sensitivity to various analytes. Figures 3 and 4 show the structure and designation of phthalocyanines and porphyrins, which were used as active layers of sensors based on the SPR phenomenon in the works described in this review.

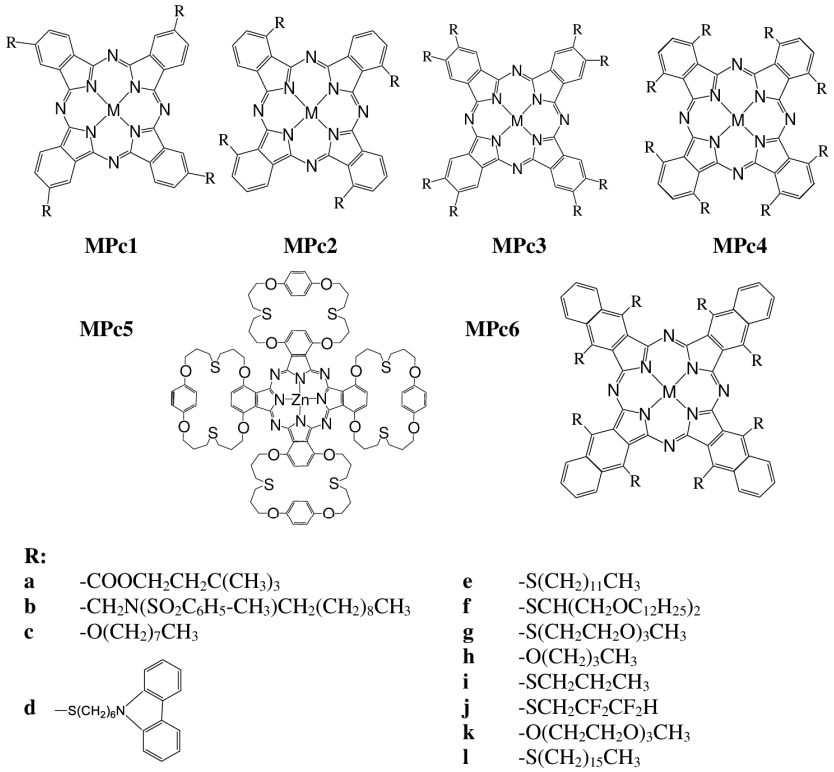

Figure 3. Scheme of metal phthalocyanines (MPc) used for the preparation of the sensing layers of SPR and TIRE sensors. M is a central metal, and R is a substituent.

Films of unsubstituted phthalocyanines and MPcs with fluorine and chlorine substituents in macrorings are usually deposited by PVD because they have very bad solubility in organic solvents but are sublime without decomposition in vacuum. There are several examples in the literature where films of unsubstituted and fluorosubstituted phthalocyanines, deposited by PVD, are used for the detection of ammonia and nitrogen dioxide. In our previous work [37], films of perfluorinated metal phthalocyanines $MPcF_{16}$ (M = Cu(II), Co(II), Zn(II), Ni(II)) were prepared by PVD to test their SPR response to gaseous NH_3 in

concentrations of 100 and 200 ppm ("parts per million", when describing the concentration of gases, 1 ppm is equal to 0.0001%). Figure 5 shows that the minimum in the SPR curve, which is directly related to the thickness and dielectric constant of the CuPcF16 film, shifts from 44.4° to 46.4° (Figure 5a) after the film exposure to NH_3 (200 ppm). The analysis of kinetic curves (Figure 5b) showed that the SPR response depended on the type of central metal and increased in the order of $NiPcF_{16}$ < $CuPcF_{16}$ < $CoPcF_{16}$ < $ZnPcF_{16}$.

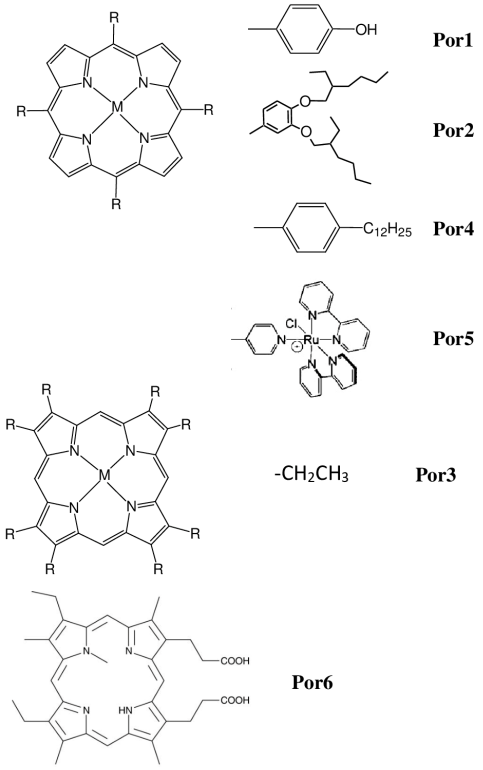

Figure 4. Scheme of porphyrins (Por) used for the preparation of the sensing layers of SPR and TIRE sensors. M is a central metal, and R is a substituent.

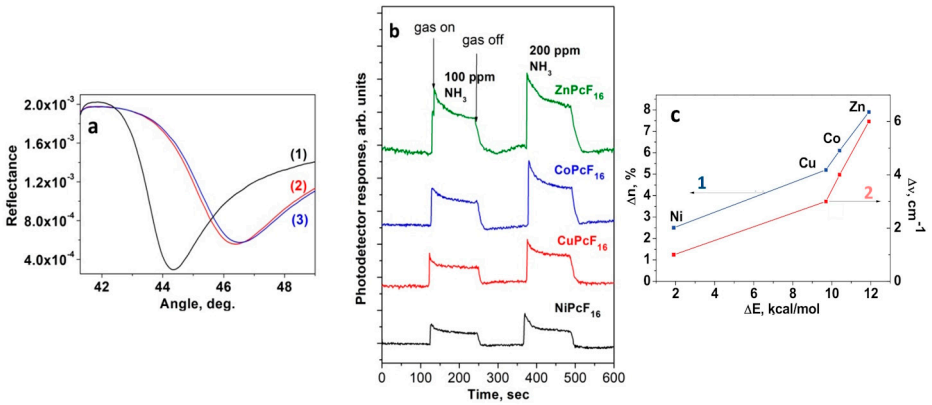

Figure 5. (**a**) SPR curves for a substrate covered with Au (1), Au/as-deposited $CuPcF_{16}$ film (2), and Au/$CuPcF_{16}$ exposed to 200 ppm NH_3 (3). SPR response curves were recorded using the wavelength of 633 nm (He–Ne laser) at a fixed angle of incidence of 44.2°. (**b**) SPR response of $MPcF_{16}$ (M = Ni, Cu, Co, Zn) films toward gaseous NH_3 (100 ppm and 200 ppm). (**c**) The change of refractive index (n) of $MPcF_{16}$ films after exposure to NH_3 vapor vs. calculated relative electronic energies (ΔE) (1, blue); the frequency shift of the IR band corresponding to the inner ring breathing (at 955, 953, 947, 937 cm^{-1} for $NiPcF_{16}$, $CoPcF_{16}$, $CuPcF_{16}$, and $ZnPcF_{16}$, respectively) vs. calculated relative electronic energies (2, red). Adapted with permission from [37]. Copyright 2016 Elsevier.

Spadavecchia et al. [38] showed that the adsorption of NH_3 molecules caused the change in UV–vis absorption spectra of $MPcF_{16}$ films and, as a consequence, the change of k. Since n and k are connected through the Kramers–Kronig relations, the refractive index (n) also changes [39]. The most noticeable changes of *n* (from 1.64 to 1.51) and *k* (from 0.26 to 0.20) upon exposure to NH_3 were observed in the case of the $ZnPcF_{16}$ film (Figure 5c). It was found that the value of the sensor response correlated well with the binding energy values obtained using DFT calculations as well as with the data from the IR spectroscopy study. Interaction with ammonia led to a shift (by 5–6 cm^{-1}) of the bands in the IR spectrum of phthalocyanine films (Figure 5c), which were associated with deformation of the inner ring, which apparently indicated the coordination of ammonia by the central atom.

Opilski et al. [40] studied nickel phthalocyanine (NiPc) layers with thicknesses from 10 to 85 nm, deposited by PVD, in the SPR sensors for NO_2 (100 ppm) and demonstrated the dependence of the SPR response on the films' thickness. The maximal sensor response was given by a 30 nm-thick layer deposited on a substrate cooled to −10 °C. The authors also mentioned that no shift in the coupling angle was observed when gases such as H_2O and CO_2 were introduced into contact with the phthalocyanine film. The authors concluded that the films had high sensitivity to gaseous NO_2, but they did not study any quantitative characteristics of the sensors.

Another group of researchers [41,42] carried out quantitative investigations of the SPR response of CoPc films to NO_2. The films were deposited by PVD onto a glass slide covered with silver. The limit of detection (LOD) was determined to be around 0.07 ppm.

For the detection of VOCs, phthalocyanines with additional ligands in the axial position or with long alkyl substituents in the aromatic ring are used because such groups provide additional active centers of interaction with analyte molecules. Evyapan et al. [43] studied the SPR response of films of chloroaluminium phthalocyanine (ClAlPc), fluoroaluminium phthalocyanine (FAlPc), and fluorochromium phthalocyanine (FCrPc) containing halogen substituents in axial positions toward acetic acid, alcohols, and amines in the concentration range of 200–1000 ppm (Figure 6). Films of these phthalocyanines were prepared by spin-coating their solution in trifluoroacetic acid. Table 1 summarizes the sensitivity and LOD of the investigated sensors. All films were shown to exhibit the maximum sensitivity to CH_3OH and CH_3COOH among the investigated vapors.

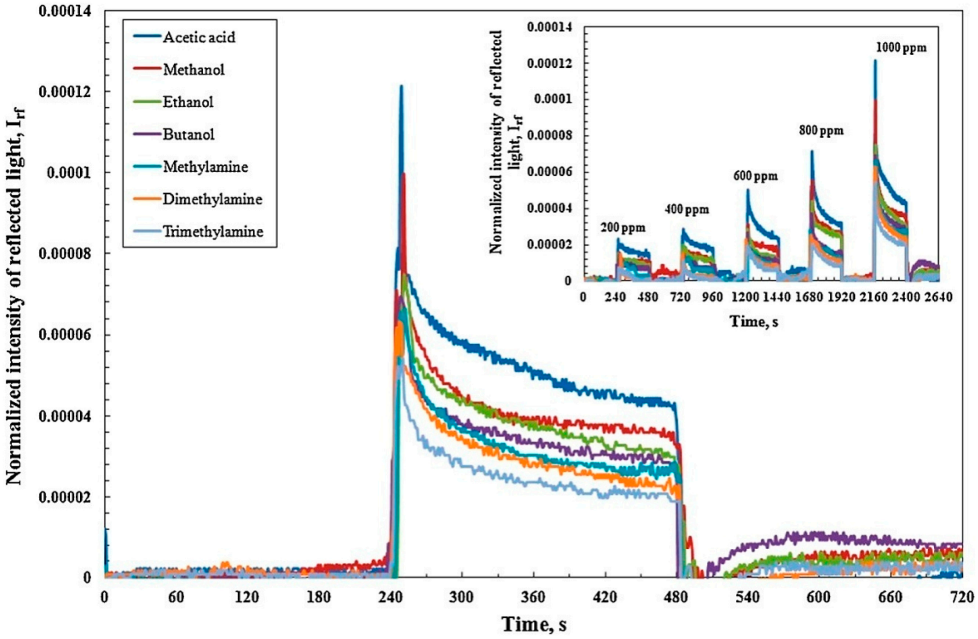

Figure 6. SPR sensor response of FAlPc spun films to various VOCs (1000 ppm) (inset: the response to five different vapor concentrations). Reprinted with permission from [43]. Copyright 2016 Elsevier.

Table 1. Sensing characteristics of MPc spun films. Reprinted with permission from [43]. Copyright 2016 Elsevier.

Analyte Vapor	S (ppm^{-1}) × 10^{-7}/LOD (ppm)		
	ClAlPc	**FAlPc**	**FCrPc**
Acetic acid	1.30/46.2	1.21/49.6	1.05/57.1
Methanol	1.01/59.4	0.99/60.4	0.85/70.5
Ethanol	0.88/67.5	0.74/80.5	0.65/91.7
Butanol	0.70/85.1	0.69/86.5	0.58/103.4
Methylamine	0.67/89.6	0.66/90.4	0.47/126.8
Dimethylamine	0.55/108.9	0.63/94.9	0.46/128.5
Trimethylamine	0.41/145.6	0.54/110.7	0.35/170.5

S is the sensitivity, determined as the change in reflected light intensity per concentration.

The penetration of analyte vapors into the film leads to its swelling, which causes both a change in the thickness of the film and its optical parameters. The authors analyzed the order of the sensor response from the point of view of the diffusion coefficient of analyte vapors during the films' swelling process. It was shown that the diffusion rate was influenced by both the size of the analyte molecule and the functional groups in the phthalocyanine molecule. Smaller analyte molecules can more easily penetrate the film. The diffusion coefficients of C_2H_5OH and C_4C_9OH are lower than those of CH_3COOH and CH_3OH. Although the size of the CH_3COOH molecule is slightly larger than that of CH_3OH, the response to CH_3COOH is higher than to other investigated VOCs. According to the authors, this may be due to the better ability of -COOH groups to form hydrogen bonds with Cl and F substituents in the axial positions of the phthalocyanines.

Another way to increase the sensitivity of VOCs is through the introduction of substituents with various functional groups. For example, films of CuPc3b were shown to have a good SPR response to benzene and chloroform vapors [44].

It was shown using the theoretical fitting of experimental SPR curves (Figure 7a) to Fresnel's equation in a modified form (Equation (1)) [30] that the exposure of CuPc3b films with benzene led to a change in their thickness from 10.39 nm to 11.45 nm and their refractive indexes from 1.6 to 1.58.

$$\Delta\theta = \frac{(2\pi/\lambda)(|\varepsilon_m|\varepsilon_i)^{3/2}\, d}{n_p\, cos\theta(|\varepsilon_m| - \varepsilon_i)^2\varepsilon}(\varepsilon - \varepsilon_i) \quad (1)$$

where $\Delta\theta$ is the SPR shift, d and ε are the thickness and complex dielectric constant of the phthalocyanine layer, respectively, $|\varepsilon_m|$ is the modulus of the real part of the dielectric constant of gold film, and ε_i is the dielectric constant of air. The exposure of CuPc3b films to chloroform led to an increase in film thickness to 11.68 nm and a decrease in the refractive index to 1.56. Thus, CuPc3b films demonstrated a higher SPR response to chloroform than to benzene vapors (Figure 7b).

Çapan and Ilhan [45] studied the SPR response of LB thin films of metal-free 2,3,9,10,16,17,23,24-octakis(octyloxy)-29H,31H phthalocyanine (H_2Pc3c) and its zinc (ZnPc3c) and copper (CuPc3c) complexes mixed with stearic acid (SA) to VOCs and compared it with the same Quartz Crystal Microbalance (QCM) sensors. The LB technique allowed the depositing of ordered homogeneous nanoscale thin films of these phthalocyanines. LB-film technology makes it possible to transfer Pc from the water-air interface to a solid substrate and, at the same time, obtain ordered homogeneous nanoscale films, controlling their molecular architecture during deposition. Several groups of VOCs were tested as analytes, among them aromatic hydrocarbons (benzene and toluene), alcohols (methanol and ethanol), and chlorinated hydrocarbons ($CHCl_3$, CH_2Cl_2, and CCl_4). It was shown that the response to saturated vapors of chlorinated hydrocarbons was noticeably higher than

that to alcohols and aromatic hydrocarbons (Table 2). The authors explained the interaction of these gases with phthalocyanine as a physical absorption through a dipole/dipole interaction or the formation of hydrogen bonds.

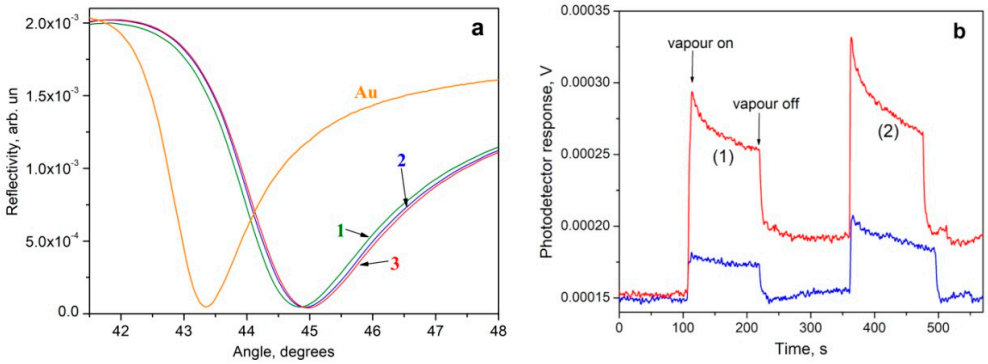

Figure 7. (**a**) SPR curves for a gold film (Au), initial gold/CuPc3b film (1), gold/CuPc3b film exposed to benzene (2), and chloroform (3). (**b**) Kinetics of the SPR response of CuPc3b films to chloroform (red line) and benzene (blue line) vapors of different concentrations: (1) $p_s/10$; (2) $p_s/5$ (p_s is the saturated vapor pressure). Reprinted with permission from [44]. Copyright 2009, Elsevier.

Table 2. Response of LB thin films in terms of the change in reflected light intensity after exposure to saturated vapors of VOCs. Prepared using the data from Ref. [45].

	H_2Pc3c/SA	**ZnPc3c/SA**	**CuPc3c/SA**
Benzene	223	259	57
Toluene	111	75	32
Methanol	178	96	33
Ethanol	93	175	26
$CHCl_3$	384	210	103
CCl_4	135	92	47
CH_2Cl_2	762	269	221

Langmuir–Blodgett films containing 2–10 layers of ZnPc1d were tested as active layers of SPR sensors for detecting dichloromethane, CCl_4, toluene, and m-xylene [46]. It was shown that the films of ZnPc1d also demonstrated a higher response to dichloromethane.

In another work [47], the same group of authors used ZnPc5 (Figure 3) bearing crown ether moieties, which are capable of host–guest interaction. Films consisting of 8, 12, 16, and 20 monolayers of ZnPc5 were produced by an LB method on gold-coated glass slides and tested as a sensing layer for the determination of chloroform. It was shown that the films consisting of 20 monolayers exhibited a higher sensor response to $CHCl_3$, with response and recovery times of 2 and 6 s (Figure 8). The LOD and sensitivity were 3.76 ppm and 0.797×10^{-3} ppm^{-1}, respectively. The same compound was also tested in SPR sensing of acetone, methanol, ethanol, and isopropanol (at saturated concentrations) [48]. It was found that among the investigated analytes, the highest SPR response was observed for acetone, which has the largest dipole moment and diffusion coefficient, which was estimated in this work.

The influence of the substituent type on the SPR response of spun films of NiPc3 bearing R = $–S(CH_2)_{11}CH_3$ (NiPc3e), $–SCH(CH_2OC_{12}H_{25})_2$ (NiPc3f), and $–S(CH_2CH_2O)_3CH_3$ (NiPc3g) to chloroform and benzene vapors was studied in the work of our research group [49]. It was shown that the SPR response to chloroform was dependent on the type of substituent and increased in the order of NiPc3e < NiPc3f < NiPc3g, while the type of substituents did not affect the response to benzene vapors. The interaction of films with organic vapors led to a change in both their thickness and optical parameters. For example,

a maximal change in thickness by 8.9% and refractive index by 2.1% was observed when a film of NiPc3g with R = –S(CH_2CH_2O)$_3CH_3$ was exposed to chloroform. The nature of the interaction between the films and gaseous analytes was studied by means of Raman spectroscopy. It was concluded that $CHCl_3$ interacted with substituents in NiPc3e g because the changes of C-H vibrations typical for the formation of hydrogen bonds C-H· · · Cl with $CHCl_3$ molecules were observed in the Raman spectra of the films in the presence of $CHCl_3$. In the Raman spectra of NiPc3e g films recorded in benzene vapors, the most prominent changes were observed in the range of vibrations of aromatic macrorings, which was an indication of π–π interaction between the phthalocyanine and benzene aromatic rings.

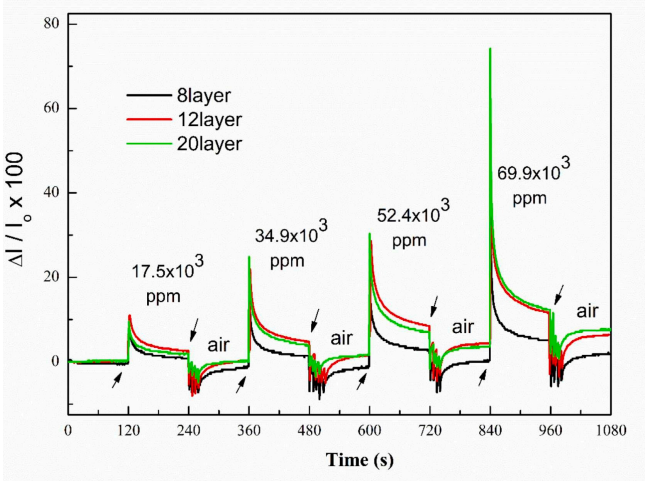

Figure 8. Kinetic response of the ZnPc5 LB thin film sensor for different concentration values of the chloroform vapor. Reprinted with permission from [47]. Copyright 2023 Elsevier.

Another group of researchers [50] also studied the effect of the substituents in the ring of CuPc4h and CuPc3c on the SPR response to chloroform, dichloromethane, and toluene vapors. The role of the expanded aromatic system was also considered using the copper naphthalocyanine derivative CuPc6c (Figure 3) as an example. Thin films of these CuPc derivatives were deposited by a spin-coating technique. The sensor response was expressed as R = $\Delta I/I_o \times 100\%$, where ΔI is the difference between the reflected light intensity values at the steady state (I) and the unexposed CuPc film (I_o). The concentration of investigated VOCs varied from 20% to 100% saturated vapor pressure. It was shown that the CuPc films demonstrated the maximal response at a thickness of 60–90 nm, which can be achieved when depositing at a rotation speed of 250 rpm. The sensor response was decreased in the order of CuPc6c > CuPc3c > CuPc4h, that is, the expansion of the aromatic ring and an increase in the alkyl substituent length led to an increase in the SPR response.

Substituted porphyrin derivatives were also shown to be used for the detection of VOCs. Evyapan et al. [51] used the SPR method for the detection of acetic acid and methylamine using Langmuir–Schaefer films of 5,10,15,20-tetrakis-[3,4-bis(2-ethylhexyloxy)phenyl]-21H, 23H-porphine (Por2, Figure 4) deposited onto 40 nm gold-coated glass substrates as active layers. The dependence of the sensor response to the vapors of acetic acid (855 ppm) and methylamine (900 ppm) on the number of layers was investigated (Table 3).

The adsorption of gaseous analytes caused the films' swelling and, as a result, an increase in their thickness. The films' sensitivities and LOD calculated as $3\sigma/S$ are also given in Table 3. All films demonstrated a better sensor response to acetic acid than to methylamine. The minimal detection limit was observed for the thicker film containing 10 layers.

Çapan and Özkaya [52] compared the SPR response of spun films of 2,3,7,8,12,13,17,18-Octaethyl-21H, 23H-porphine (Por3, Figure 4) and 2,3,7,8,12,13,17,18-Octaethyl-21H, 23H-porphine zinc(II) porphyrins (ZnPor3) to saturated vapor of chloroform and acetone. It was shown that metal-free porphine demonstrated a higher response to both chloroform

and acetone compared to that of ZnPor3. The authors explained this result by the reduced π-stacked aggregation of the molecules in ZnPor films. A comparative study of the Por3 films obtained by spin coating and Langmuir–Blodgett methods showed that the SPR response to chloroform, benzene, toluene, and methanol was higher in the case of LB films exhibiting larger surface areas [53].

Table 3. SPR analysis of thin films of Por2. Adapted with permission from [51]. Copyright 2018 Elsevier.

	4 Layers		**6 Layers**		**8 Layers**		**10 Layers**	
Thickness of LS films (Å)	66		151		238		314	
Analyte vapors	Acetic acid	Methyl-amine	Acetic acid	Methyl-amine	Acetic acid	Methyl-amine	Acetic acid	Methyl-amine
Swelling time (s)	147	388	214	480	285	483	334	654
SPR shift after exposure ($\Delta\theta^{\circ}$)	0.35	0.15	0.95	0.30	1.00	0.55	1.95	0.70
Thickness change after exposure (Å)	~15	~7	~39	~12	~41	~18	~81	~24
S (ppm^{-1}) × 10^{-7}	1.50	0.55	3.18	1.50	5.52	2.76	9.82	4.38
LOD (ppm)	40.08	108.00	18.86	40.00	10.87	21.77	6.11	13.71

Çapan [54] compared the SPR sensor response of LB thin films of zinc porphyrin (Por4, Figure 4) to benzene and ethyl benzene, toluene, and xylene. It was shown that the films demonstrated a higher sensitivity to benzene due to its higher volatility, a lower molar volume, and a relatively high viscosity parameter, which, according to the authors' opinion, led to easier penetration of benzene molecules into the sensing layer.

2.2. MOSPR Sensors

Manera et al. [21,55,56] suggested an original method of magneto-optical SPR (MOSPR), which was based on the combination of magneto-optical effects and SPR excited in multilayer structures of noble (Au or Ag) and ferromagnetic metals (e.g., Co or Fe) (Figure 9). The applicability of this method to control changes in the refractive index at the metal–dielectric interface has been demonstrated.

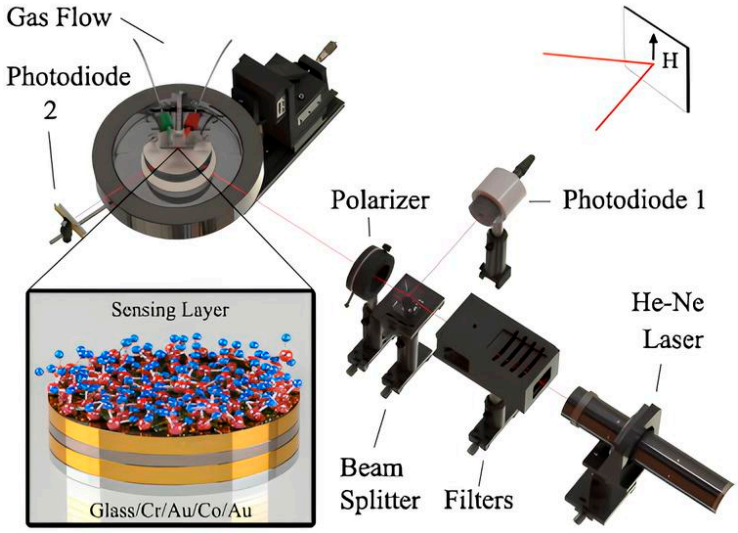

Figure 9. Experimental setup for SPR and MOSPR characterization in dry air and a controlled atmosphere. The magnetic field vector is represented; it is applied in the plane of the surface and perpendicular to the plane of incidence of light. Reprinted with permission from [55]. Copyright 2013 Elsevier.

This MOSPR technique was based on a magneto-plasmonic (MP) modulation produced in multilayers of noble and ferromagnetic metals. The combination of these metals led to a noticeable enhancement of the MO Kerr effects of p-polarized light when the SPR condition was met. Such enhancement significantly depends on the excitation conditions and, therefore, on the refractive index of the dielectric, which is in contact with the metal layer. In a traditional SPR sensor, the metal layer (Ag or Au) acts as the transducing layer, while in the MOSPR technique, this role is played by a magneto-plasmonic multilayer structure consisting of noble metal and ferromagnetic layers of suitable thickness. The MOSPR sensor signal is determined as the relative variation in the reflected p-polarized light, defined as $\Delta R = R(+M) - R(-M)$, where R ($\pm M$) is the reflectance of the p-polarized light with the sample magnetically saturated along the direction of the applied magnetic field. For the measurements of magneto-optical activity upon plasmon excitation, an electromagnet was installed in a transversal configuration, which changes the magnetization of the Co layer between its saturation states. The principles of this method were described in detail by Gonzalez-Diaz et al. [57]. The MOSPR technique allowed the researchers to draw some conclusions about changes in the optical anisotropy of the investigated sensing layers, which was important not only to investigate the sensor response but also to find correlations between optical and structural properties.

The authors of [21,58] used this technique for monitoring optical and morphological changes in the LS layers of Zn(II) and Co(II) porphyrins upon their interaction with VOCs and amines. Films of ethane-bridged zinc bis-porphyrin (ZnPP with R = -CH_2CH_3, Figure 10) were deposited by the horizontal lifting or LS technique onto magnetoplasmonic substrates. The prepared films were exposed to nitrogen-containing analytes, viz. n-butylamine and aniline vapors as well as NH_3 gas in dry air. The response of similar ethane-bridged bis-porphyrin of Co(II) to methanol, ethanol, and isopropanol using the same method was studied in another work by the same group of authors [59]. The investigated dimeric porphyrins incline toward a conformational change when interacting with the analytes (Figure 10) [60].

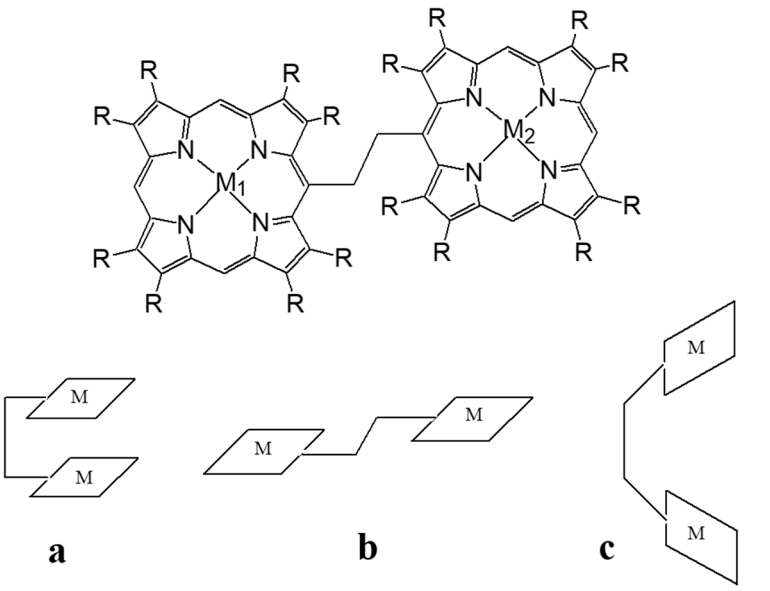

Figure 10. Structure of syn- (**a**), anti- (**b**), and tweezer (**c**) conformers of bis-porphyrins (MPP). R = -CH_2CH_3.

SPR and magneto-optical curves of ZnPP films on an Au/Co/Au multilayer before and during interaction with aniline vapors are shown in Figure 11.

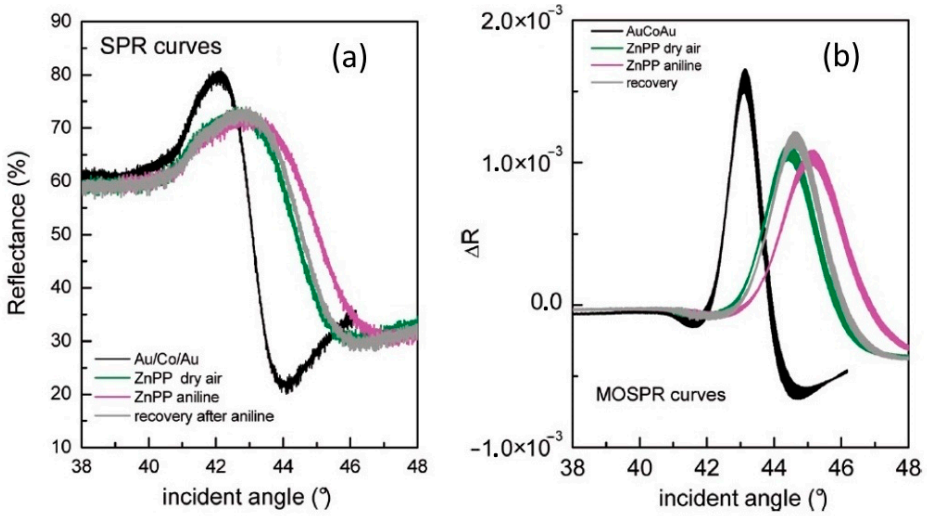

Figure 11. SPR (**a**) and magneto-optical (**b**) curves showing the change in optical features of the Au/Co/Au multilayer after deposition of the ZnPP LS thin films and after its interaction with saturated aniline vapors. Recovery of the sensing surface is also evidenced. Reprinted with permission from [21]. Copyright 2012, American Chemical Society.

The adsorption of amines on the surface of the ZnPP layer led to a change in its optical properties and the plasmon wave vector, which, in turn, translated into the angular shift of both the SPR and MOSPR curves.

The same group of authors [56] also used the layers of the ZnPP derivative to compare their SPR and MOSPR sensor responses to n-butylamine and di-butylamine vapors. SPR and MOSPR sensor responses to di-butylamine were higher than those to n-butylamine, the response and recovery times were also shorter in the case of the secondary amine (Table 4). The better sensitivity to the secondary amine was explained by their electron-donating power and, as a consequence, by the increase in the bond strength of di-butylamine with the active site of the porphyrin films.

Table 4. Comparison of gas sensing parameters of the sensors based on ZnPP investigated by SPR and MOSPR techniques. Adapted with permission from [55]. Copyright 2013 Elsevier.

Technique	Analyte	Sensitivity (ppm^{-1})	LOD (ppm)	t_{resp} (min)	t_{rec} (min)
SPR	n-butylamine	2.32×10^{-6}	14,200	10	8
	di-butylamine	4.32×10^{-5}	760	3	6
MOSPR	n-butylamine	5.23×10^{-6}	5100	12	9.7
	di-butylamine	4.31×10^{-4}	60	3	7.5

The MOSPR method allowed recording the higher signal-to-noise ratio sensorgram and, as a result, provided better characteristics, such as sensitivity, signal-to-noise ratio, and LOD, than the traditional SPR. For instance, the LOD of di-butylamine was 60 ppm in the case of the MO-SPR method, whereas it was 760 ppm in the case of SPR.

The same group of authors [58] compared the MOSPR sensor response of CoPP (Figure 10) and bisphthalocyanine of terbium $Tb(Pc(OC_{11}H_{21})_4)_2$. To prepare a MOSPR sensor for the detection of n-butylamine, their films were deposited by the LS method onto Au/Co/Au magneto-optical transducers. It was found that, like CoPP, $Tb(Pc(OC_{11}H_{21})_4)_2$ films demonstrated a good MOSPR response to n-butylamine. The sensitivity of the MOSPR sensor depended on the overlap between the plasmonic probe energy and the electronic absorption transitions of the studied complexes. Sensitivity to the detected

n-butylamine increased when the propagating plasmonic energy was in resonance with the HOMO–LUMO transitions of the investigated macrocyclic derivatives.

2.3. TIRE Sensors

Another optical technique that is based on the SPR phenomenon is Total Internal Reflection Ellipsometry (TIRE). This technique combines ellipsometry in total internal reflection mode and the SPR phenomenon [61–64]. This technique can be realized as an extension to the commercial spectroscopic ellipsometer (Figure 12a, elements 1–5) and is comprised of a 45° prism and gold-coated glass slide, which were brought into optical contact via index matching fluid. The experimental flow cell was attached to the slide with a deposited active layer [44].

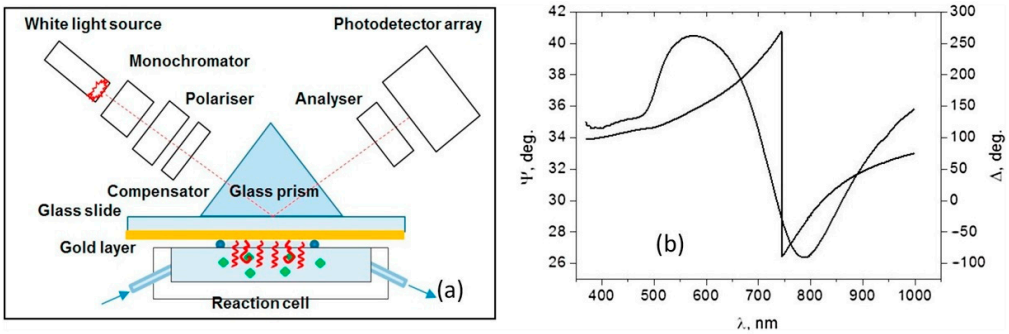

Figure 12. (**a**) Total internal reflection ellipsometry experimental set-up; (**b**) typical TIRE spectra of Cr/Au films. Reprinted with permission from [63]. Copyright 2019 Elsevier.

Unlike SPR, which measures the p-polarized light intensity, the TIRE method gives the spectra of two ellipsometric parameters, Ψ and Δ. The spectra of Ψ, representing the ratio of the amplitudes of polarized light ($tn(\Psi) = A_p/A_s$), are very similar to the SPR curves. While the spectra of Δ, representing the phase shift between p and s components ($\Delta = \varphi_p - \varphi_s$), look like a sharp (almost vertical) drop of the phase from 2700 to −900 near the plasmon resonance (Figure 12b). For this reason, the TIRE method demonstrates better sensitivity than the SPR one.

As in the SPR technique, films of metal phthalocyanine with long alkyl substituents are used as active layers. For example, films of CuPc3b with bulky substituents (R = $-N(SO_2C_6H_5–CH_3)CH_2(CH_2)_8CH_3$ spun onto a gold-coated slide were tested in the sensor layer for the detection of benzene and chloroform [44]. Ψ and Δ spectra of CuPc3b films and the same films after exposure to these analytes are shown in Figure 13. The larger change of the film thickness (difference of 0.39 nm) and the higher Δ shift (from 530.1 to 525.3 nm) in the case of $CHCl_3$ compared to those in the case of benzene exposure (from 525.3 to 523.7 nm) testified to the higher sensitivity of the CuPc3b films to $CHCl_3$.

A more detailed study of the performance of TIRE sensors was carried out in our work using films of octa-substituted zinc phthalocyanines bearing nonfluorinated (ZnPc3i) and fluorinated (ZnPc3j) n-propanol substituents in peripheral positions as optical membranes to determine trimethylamine vapor (10–300 ppm) [65]. Exposure to 100 ppm $N(CH_3)_3$ led to a noticeable Δ shift (Figure 14a,b), which was the result of a change in the optical parameters (n and k) (Figure 14c,d). The Δ shift was much smaller in the case of ZnPc3i films, which indicated their lower sensitivity to the investigated amine. The LOD of $N(CH_3)_3$ was calculated to be 20 ppm in the case of ZnPc3j film. A higher value of the binding energy between ZnPc3j and $N(CH_3)_3$ molecules (−1.151 eV) compared to that between ZnPc3i and $N(CH_3)_3$ (−1.093 eV), obtained as a result of DFT calculations, correlated well with the higher sensor response of ZnPc3j to $N(CH_3)_3$.

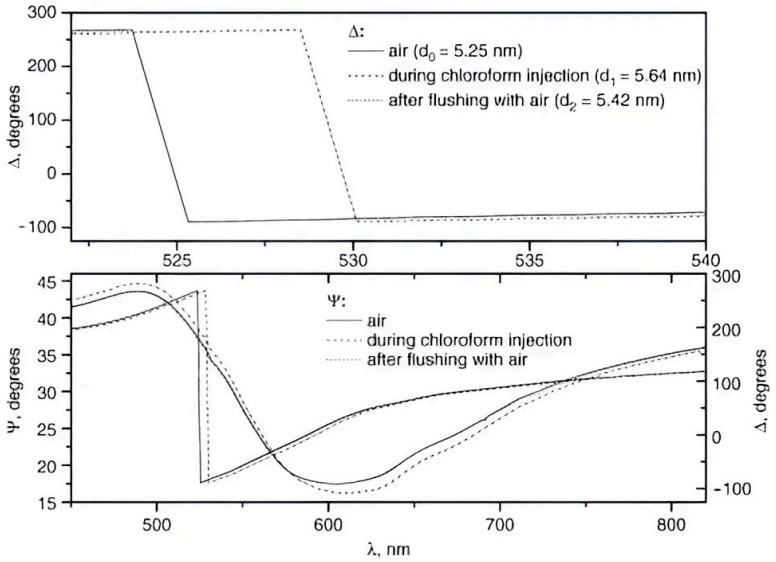

Figure 13. $\Psi(\lambda)$ and $\Delta(\lambda)$ TIRE spectra of CuPc3b-coated Cr/Au films. The effect of exposure to chloroform vapor. The enlarged section of the $\Delta(\lambda)$ spectrum is shown above. Reprinted with permission from [44]. Copyright 2009, Elsevier.

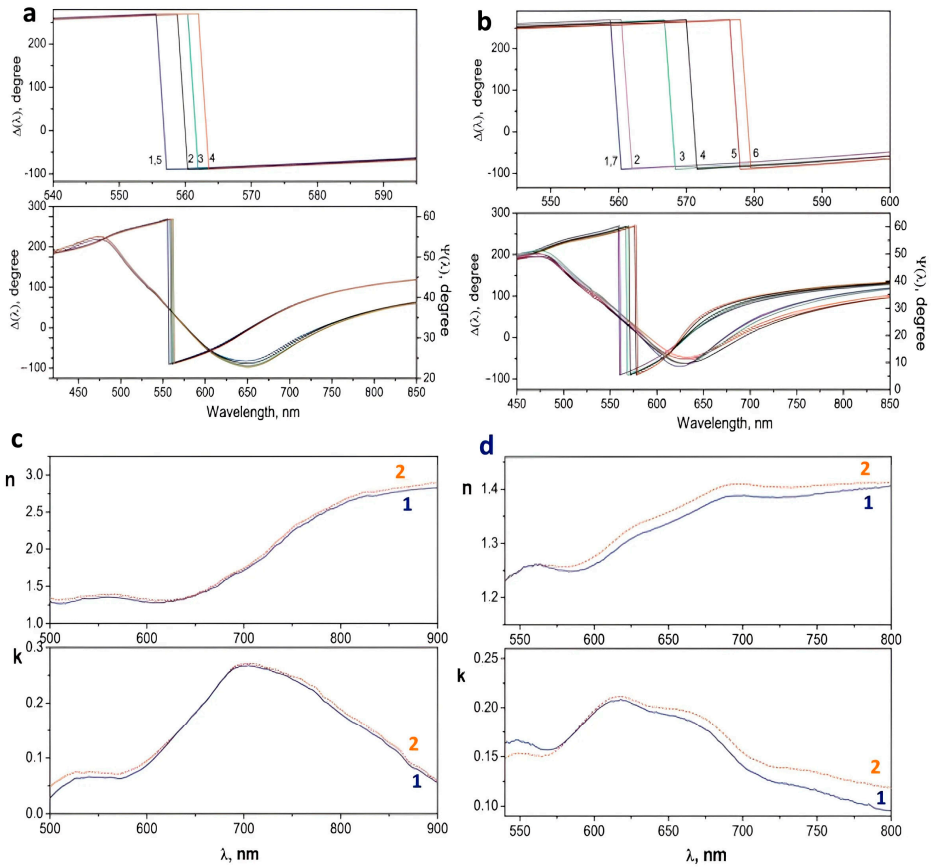

Figure 14. $\psi(\lambda)$ and $\Delta(\lambda)$ TIRE spectra: (**a**) ZnPc3i in air (curve 1); after injection of trimethylamine 200, 250, and 300 ppm (curves 2, 3, and 4, respectively); after flushing with air (curve 5); (**b**) ZnPc3j in air (curve 1); after injection of trimethylamine 20, 60, 100, 250, and 300 ppm (curves 2–6, respectively); after flushing with air (curve 7). Enlarged sections of the $\Delta(\lambda)$ spectra are shown at the top. Variation in the refractive index (n) and extinction coefficient (k) of (**c**) ZnPc3i and (**d**) ZnPc3j films exposed to air (solid lines, 1) and trimethylamine (dotted lines, 2) at a concentration of 100 ppm. Reprinted with permission from [65]. Copyright 2015, Elsevier.

3. Phthalocyanine- and Porphyrin-Based SPR Sensors for the Detection of Analytes in Solutions

Sensors based on the SPR phenomenon can be used not only for the detection of gaseous analytes but also for the determination of various compounds in solutions [66–69]. There are several examples of the application of porphyrin and phthalocyanine-based SPR sensors in the literature.

Among porphyrins, bisporphyrins with an ethane bridge are of great interest due to their ability to change conformations from syn- to anti-form or to a tweezer-type geometry (Figure 10), depending on the chemical medium, changing the electronic absorption spectra [70–72]. Bettini et al. [60] tested LS films of bis-porphyrin compounds described above (Figure 10) with different central metals (Ni and Cu) as active layers of SPR sensors for the detection of histidine in water solutions. It was shown that the molecules in aggregated species of LS films were mostly in the syn-form (Figure 10), whereas in the histidine media, the molecules underwent the conformational switch into the anti-form. This was reflected in the bathochromic shift of the Q-band by 15 nm in the case of CuPP and the hypsochromic shift by 5 nm in the case of NiPP. The corresponding shifts of the SPR curves are shown in Figure 15. NiPP films were sensitive to histidine in the concentration range from 10^{-4} to 10^{-6} M, while CuPP films demonstrated the capability to detect histidine down to nanomolar concentration. The authors associated these different effects produced by histidine on NiPP and CuPP with the different spatial architectures of these metalloporphyrins, namely the predominant planar structure of the CuPP complex and the tetrahedral distorted structure of NiPP. It was also shown that the films of the CuPP complex can be used for the detection of histidine in the presence of arginine.

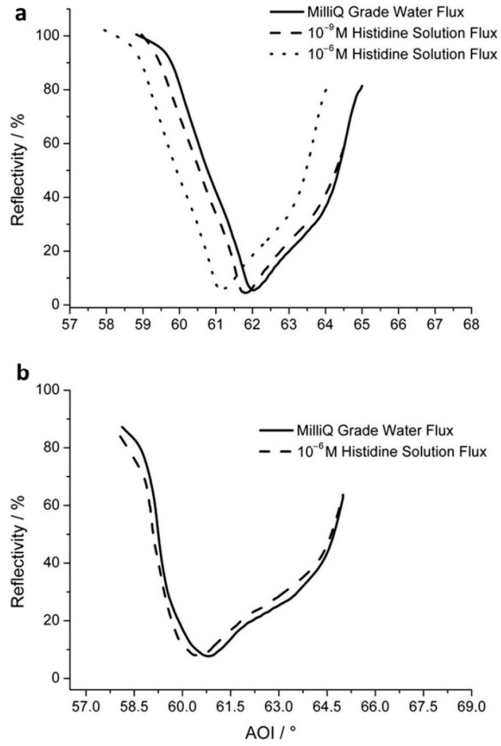

Figure 15. SPR curves obtained for the CuPP film (**a**) and NiPP film (**b**) upon MilliQ-grade water and histidine solution fluxing. Reprinted with permission from [60]. Copyright 2019 Elsevier.

Thin films of another bisporphyrin (Figure 10, M_1 = 2H, M_2 = Cu) were deposited by the LS technique using pure water as a subphase to test them as active layers in SPR sensors to detect aniline at low concentrations up to 1 nM in aqueous solution [73]. It was found that in order to induce the *syn*-to-*anti* conformational change in this bisporphyrine, the simultaneous presence of an amino group and an aromatic ring in the analyte molecule

was necessary. The films showed no optical response to either aliphatic amines or phenols, which indicated a cooperative effect of the amine and aromatic groups. At the same time, the films were sensitive to α-methylbenzylamine and *N*-methylphenethylamine, but the SPR response to these analytes was less than to anyline.

The combination of SPR with other physical methods, e.g., spectroscopy, electrochemistry, chromatography, and mass spectrometry, makes this method more powerful [74]. For example, SPR combined with electrochemistry is used for simultaneous monitoring of the change in electrochemical parameters and refractive index of the active surface in order to study various reactions at the interface [75].

Munoz et al. [76] employed SPR in combination with cyclic voltammetry to study the electrochemical oxidation of acetaminophen, dopamine, and catechol. For this purpose, they deposited a Zn(II) porphyrin derivative bearing electrochemically active substituents (Por5, Figure 4) on the gold surface. Simultaneous variation of the SPR angle and cyclic voltammetry recording made it possible to register changes in the electronic states of adsorbed molecules. A graph of the dependence of the SPR reflection angle on the applied potential at a Por5/Au interface in a pure electrolyte and in the presence of analytes is shown in Figure 16. It can be seen that the SPR signal increases in the presence of catechol and dopamine, indicating that they interact more effectively with the film by changing the electron density at the Por5/Au interface. The authors explained this by the π-π interaction of the aromatic ring of these phenolic derivatives with the porphyrin macrocycle. Such an interaction may be sufficient to slow down the diffusion of electroactive molecules from the electrode surface and reduce them to sufficient cathode potentials. In addition, the electrocatalytic reaction can have an effect on the molecular interface.

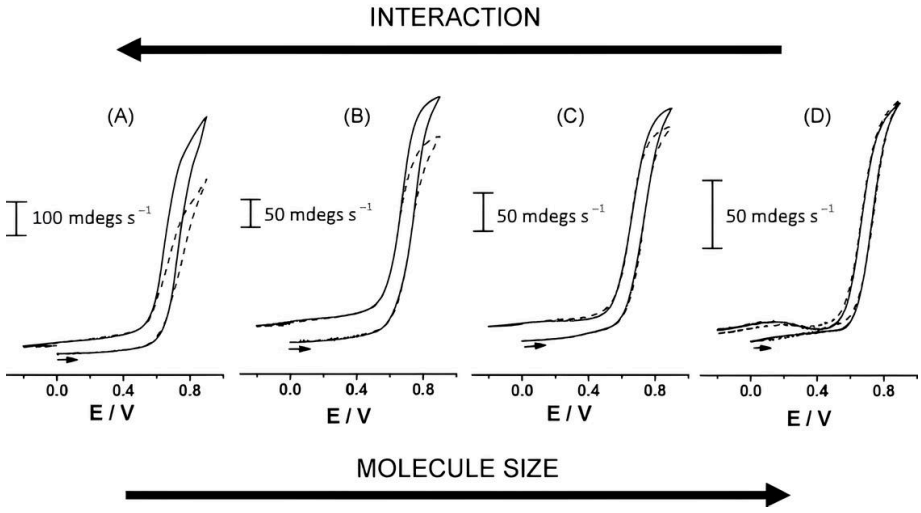

Figure 16. Dependence of the SPR reflection angle on the applied potential at a Por5/Au interface in pure 0.1 M $NaClO_4$ electrolyte solution (dashed line) and in the presence of 100 M (solid lines) of (**A**) catechol, (**B**) dopamine, (**C**) acetaminophen, and (**D**) ferrocyanide. Reprinted with permission from [76]. Copyright 2009, Elsevier.

In addition to toxins and hazardous substances, porphyrin films are also used to detect biomolecules and bacteria and to study interactions with peptides and DNA [77,78]. For example, Perenon et al. [79] studied the interaction of N-methyl mesoporphyrin IX (Por6, Figure 4) with DNA by SPR. It was shown that N-methyl mesoporphyrin IX interacts more strongly with a parallel G4 structure than with an antiparallel one. Zangenehzadeh et al. [80] demonstrated the performance of self-assembled monolayers (SAMs) of *meso*-pyridyl porphyrin, 5-(4-(2-(4-(*S*-acetylthiomethyl)phenyl)ethynyl)phenyl)-10,15,20-tris(4-pyridyl)porphyrin on a gold substrate to capture *Escherichia coli* (*E. coli*) bacteria and studied the stability and repeatability of their SPR response.

4. Hybrid Materials of Phthalocyanines and Porphyrins with Carbon Nanotubes and Other Porous Media

One of the most widely used approaches to increasing the sensitivity of sensors is the preparation of active layers with a porous structure. In this connection, hybrid materials of metal phthalocyanines with carbon nanomaterials [6,81], oxides [82,83], polymeric membranes [84], and silica matrix [85] are very promising due to their high surface area-to-volume ratio. Some of them were successfully used in SPR sensors.

Hybrids of metal phthalocyanines and porphyrins with such carbon nanomaterials as carbon nanotubes, nanohorns, graphite, graphene, and their derivatives are widely used in various chemical sensors, especially resistive and electrochemical ones [6,86–88]. To obtain hybrid materials, nanocarbon materials are modified with phthalocyanines and porphyrins by both covalent and non-covalent functionalization [81].

There are not many works on the use of hybrid materials with nanotubes modified with polyaromatic molecules in SPR sensors in the literature, but their analysis shows that these materials exhibit good sensor performance and can be successfully used for the analysis of both gaseous analytes and for the determination of various substances in solutions. For example, a quite interesting result was obtained by Banimuslem et al. [89]. The researchers used hybrid materials of single-walled carbon nanotubes (SWCNT) functionalized with phthalocyanines bearing long alkyl substituents as active layers of TIRE sensors. The TIRE response was compared with the layers of CuPc/SWCNT with R = -O(CH_2CH_2O)$_3CH_3$ or -S(CH_2CH_2O)$_3CH_3$ introduced in different positions of the phthalocyanine ring, viz. peripheral (CuPc1g, CuPc1k) and non-peripheral (CuPc2g, CuPc2k) (Figure 3). The sensitivity of the layers of these four types of hybrids to methylamine, dimethylamine, and trimethylamine is compared with that of the films of the corresponding CuPc derivatives in Figure 17. It can be seen that the sensitivity of the hybrids turned out to be higher than the sensitivity of the initial copper phthalocyanines (Figure 17). The minimal LOD of methylamine, dimethylamine, and trimethylamine (3.6, 4.4, and 6.4 ppm, respectively) was found for the layer of SWCNT/CuPc1k hybrid with R = -O(CH_2CH_2O)$_3CH_3$ in peripheral positions. The response time was no more than 136 s for such types of sensors, while the recovery time varied from 150 to 191 s. The lower sensitivity to secondary and tertiary amines compared to methylamine was explained by that the steric hindrance led to a smaller number of amine molecules interacting with the active film surface.

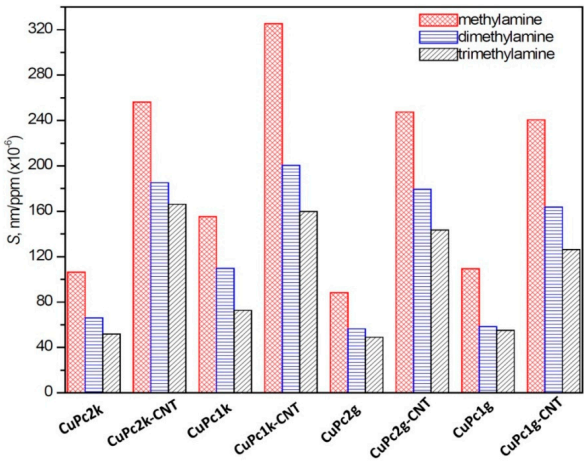

Figure 17. Sensitivity of Cu(II) phthalocyanines and their hybrids with SWCNT active layers for methylamine, dimethylamine, and trimethylamine. Sensitivity (S) was evaluated using the equation $S = \frac{1}{\Delta_o}\frac{1}{m}\sum_{i=1}^{m}\frac{\partial\Delta}{C_i}$, where $\delta\Delta$ is the change in the Δ spectra under analyte concentration (C_i), m is the number of different concentrations used in the study, and $\Delta_\circ$ is the initial change in the phase shift spectra (before exposure to amine vapors). Reprinted with permission from [89]. Copyright 2015, Elsevier.

Hybrid materials of phthalocyanine derivatives with carbon nanotubes were also used for the detection of hazardous substances in water media. If carbon nanotubes themselves do not give a sensor response when examined by the SPR method, then their hybrid materials with phthalocyanines exhibit a significant SPR sensor response when interacting with analytes, which is even higher than the response of films of those phthalocyanines that are used to modify the nanotubes. For example, the phthalocyanine CuPc2g (Figure 3) and its hybrid with acid-treated SWCNT were used for the detection of benzo[a]pyrene in water [90,91]. For this purpose, the films were drop-casted onto the slide covered with gold and then dipped into pure water or a water solution of benzo[a]pyrene (6.2 μg/L) to demonstrate the changes of $\psi(\lambda)$ and $\Delta(\lambda)$ TIRE spectra. The response of the layer of the hybrid material was found to be two times larger than in the case of CuPc2g films (Figure 18). The higher sensitivity of the hybrid film to benzo[a]pyrene is apparently due to the large number of adsorption sites available for the analyte molecules on the surface of the SWCNT/CuPc2g layer, which is associated with a large surface area-to-volume ratio compared with the CuPc2g film.

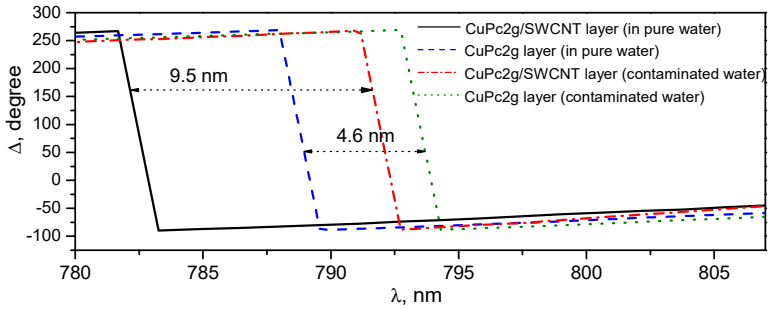

Figure 18. $\Delta(\lambda)$ TIRE spectra of a CuPc2g film in water (dashed line), after injection of benzo[a]pyrene saturated solution (dotted line), and a layer of CuPc2g/SWCNT hybrid in water (solid line), after injection of benzo[a]pyrene saturated solution (dashed-dotted line).

A similar increase in the sensor response of hybrid layers compared to pure phthalocyanine films was also observed when investigating the TIRE sensors toward pesticides (pentachlorophenol (PCP), 2-chlorophenol (2CP), diuron, and simazine) in water [92,93]. The hybrids were prepared by non-covalent functionalization of acid-treated SWCNT with CuPc1l bearing R = $-S(CH_2)_{15}CH_3$. The pesticides were examined in concentration ranges from 0.5 to 25 μg/L. The phase shift $\Delta(\lambda)$ of SWCNT/CuPc1l layers and sensitivity were 1.2–2 times larger than those of pristine CuPc1l films (Figure 19); the layers were completely recovered after washing the cell with clean water. The limits of detection of PCP, 2CP, diuron, and simazine were found to be 0.69, 0.44, 0.75, and 1.34 μg/L, respectively.

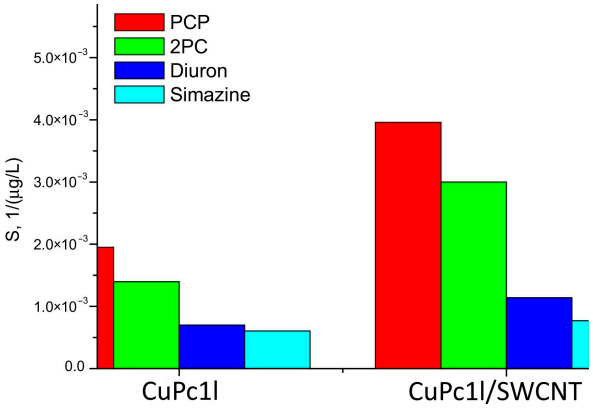

Figure 19. Sensitivity of CuPc1l and CuPc1l/SWCNT active layers to PCP, 2PC, diuron, and simazine. Reprinted with permission from [92]. Copyright 2016 Elsevier.

The interactions leading to the phase shift were both due to interactions between the aromatic rings of CuPc derivatives and pesticide molecules and van der Waals interactions between substituents in the phthalocyanine ring and chlorine atoms of pesticides. The higher sensitivity of CuPc films to pentachlorophenol than to other pesticides seems to be due to the greater number of Cl atoms in the PCP molecule.

In addition to hybrid materials with carbon nanotubes, composite materials of porphyrins and phthalocyanines with metal nanoparticles are also used to produce active layers of SPR sensors. Zhu et al. [94] developed a nanonetwork of pyridinium porphyrin-mediated calix [4]arene-functionalized AuNP composites (Apt/PyP-pSC4-AuNPs) for the creation of ultrasensitive SPR sensors for the detection of B-type natriuretic peptide (BNP). To prepare the nanonetwork, AuNPs modified with para-Sulfonatocalix [4]arene pSC4 were incubated with pyridinium porphyrin and then mixed with BNP-specific aptamers. The prepared sensing platform, based on the bionanonetworks, induced localized SPR and a large refractive index for different concentrations of BNP. The linear concentration range was from 1 to 10,000 pg/mL (R^2 = 0.9852), while the LOD was 0.3 pg/mL. The detection recovery was in the range of 92.13 to 108.69%. It was shown that the response to BNP was much higher than to bovine hemoglobin, ascorbic acid, ovalbumin, and bovine serum albumin.

Porous, fibrous membranes can also be prepared with polymers. Y.-Y. Lv and colleagues [95] studied films of composites of a zinc porphyrin covalently bound with polyimide, as shown in Figure 20a.

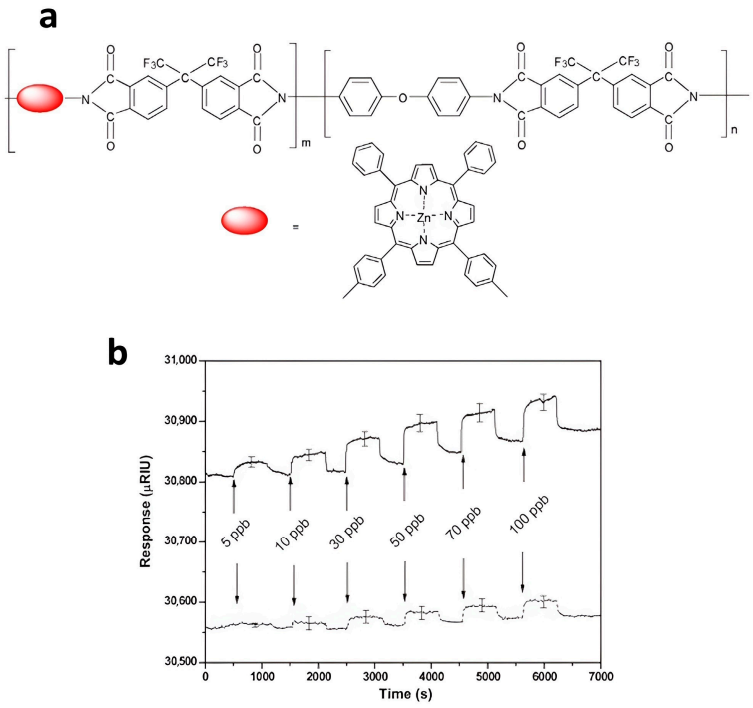

Figure 20. (**a**) Scheme of a composite based on a zinc porphyrin covalently bound with polyimide. (**b**) SPR response induced by the porphyrinated nanofibrous membrane (solid line) and dense film (dashed line) deposited on SPR chips when exposed to TNT solution with different concentrations. The average densities of the porphyrinated nanofibrous membrane and dense film coated on SPR chips are 2.17 μg cm^{-2} and 6.98 μg cm^{-2}, respectively. Reprinted with permission from [95]. Copyright 2013 Elsevier.

To prepare sensing layers for the detection of 2,4,6-trinitrotoluene (TNT) in water, the resulting polymer was deposited using electrospinning [96] and standard spin coating techniques. The effect of the deposition technique on the sensor response was investigated. It was shown that the films obtained as a result of electrospinning deposition were porous nanofibrous membranes, while spun films had dense structures. Due to the large surface

area-to-volume ratio, the electrospun films demonstrated a better sensor response to TNT and were sensitive to its low concentration up to 5 ppb (Figure 20b). At the same time, the spun films exhibited only a neglectable signal at this concentration.

Composite materials with titanium and silicon oxides are also prepared to increase the surface area of the sensor layers. For example, Rella et al. [97] used a hybrid structure of TiO_2 with MPc1a (M = Fe, Pd, Cu) (Figure 3) to determine NO_2. TiO_2/MPc1a thin films were prepared by a sol-gel method with subsequent annealing at 80 °C to carry out SPR studies in angular modulation of the response toward NO_2. The measurements of the variation in the reflectivity close to the resonance angle were performed using 20–50 ppm of NO_2 gas in a controlled atmosphere (Figure 21). The authors demonstrated the applicability of the prepared hybrid films for the SPR detection of NO_2 but did not carry out detailed investigations of the sensor performance.

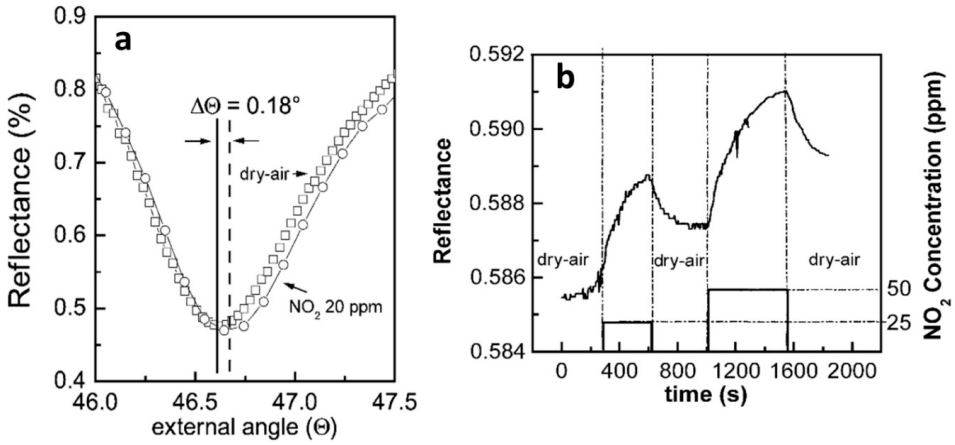

Figure 21. (**a**) SPR curves of a TiO_2/FePc1a layer in the presence of dry air flux and in ambient air containing 20 ppm NO_2 gas. (**b**) Dynamic response measured in the presence of different concentrations of NO_2 gas for a sol-gel TiO_2/PdPc1a film. Reprinted with permission from [97]. Copyright 2002, Elsevier.

Berrier et al. [98] reported on a manner of sensing NO_2 (290–6000 ppb) by SPR using a layer of 5,10,15,20-tetrakis(4-hydroxyphenyl)-21H,23H-porphine (Por1, Figure 4) embedded in a nanoporous silica matrix (NPS), which was then deposited on an Au film. The authors compared the sensitivity of four different samples to NO_2: (1) a Por1 layer (10 nm), (2) a layer of Por1 embedded in the NPS matrix (65 nm), (3) a thicker layer of Por1 embedded in the NPS matrix (130 nm), and (4) a layer of Por1 embedded in the ethylcellulose (EC) matrix (65 nm). The results of the investigation of the sensing behavior of the prepared samples by the methods of attenuated total internal reflection (ATR) in the Kretschmann configuration in comparison with the specular reflectance (Refl) measurements are summarized in Table 5. It was shown that the change in reflectance (ΔR) of the film containing only Por1 was very weak, while in the case of 65 nm thick Por1 films embedded in NPS, ΔR was 17% after the interaction with 700 ppb of NO_2 and 3% after the interaction with 350 ppb of NO_2. An increase in the film thickness to 130 nm led to an increase in ΔR to 14%. ΔR of Por1 embedded in the polymeric matrix was 700 ppb, and NO_2 was only 2%. It means that due to the high porosity, the nanoporous silica as an embedding matrix leads to an increase in sensor sensitivity to NO_2 compared to a low porous polymer matrix.

Table 5. Comparison of the reflectance changes as a function of the experimental conditions of the sample thickness, matrix, presence of porphyrin molecules, gas concentration, and optical method. Adapted with permission from [98]. Copyright 2011, Elsevier.

Sample	Layer Thickness (nm)	Matrix	NO_2 (ppb)	Optical Method	ΔR (%)
(1) Por1 layer	10	None	6000	ATR	1.5
(2) Por1 in NPS	65	NPS	700	ATR	17
(2) Por1 in NPS	65	NPS	700	Refl	8
(2) Por1 in NPS	65	NPS	350	ATR	3
(3) Por1 in EC	130	NPS	350	ATR	14
(4) Por1 in EC	65	EC	700	Refl	2

NPS—nanoporous silica matrix; EC—ethylcellulose; Refl—reflectance; ATR—attenuated total reflectance; ΔR—variation of reflectance at a wavelength of 680 nm and at the angle corresponding to the minimum reflectance of the unexposed sample.

5. Phthalocyanine and Porphyrin-Based MOFs

Metal-organic frameworks are a class of hybrid crystalline porous materials consisting of metal ions or clusters bonded to each other by organic linkers. The chemical variability, large pore volume, and internal surface area of the frameworks make them an ideal platform for creating functional materials for a wide range of applications, including chemical sensors [99,100]. Liu et al. [17] summarized the works devoted to the applications of porous polymeric structures based on tetrapyrrole compounds in electrochemical, colorimetric, fluorescence, chemiresistive, and QCM sensors.

In recent years, a direction related to the study of 2D materials in plasmon structures has been developing [101]. SPR platforms based on various MOFs can amplify the sensor response, therefore extending its applications from the detection of biomolecules to VOC sensing [64,102–104].

It was shown that a two-dimensional MOF based on metal porphyrin derivatives can be used as an SPR sensitizer [105,106]. Among other 2D materials like graphene, molybdenum disulfide, and others, 2D MOFs are characterized by a highly ordered structure with a large specific surface area and possess good electrical conductivity, high mobility of charge carriers, and efficiency of photogenerated carriers that enhance the electric field excitation and the surface plasmon resonance of the sensing interface. Apart from these, 2D MOFs can enhance the absorption of incident light, thereby improving the output signal. In addition, due to their lamellar-ordered structure, their own surface plasmon waves are coupled with the SPR of the gold film. All these properties contribute to improving the characteristics of the SPR sensor.

There are several examples of the use of porphyrin-based 2D MOF as an SPR sensitizer in the recent literature. For example, Wang and co-authors [106] demonstrated that MOF synthesized from tetra(4-carboxyphenyl)porphine (TCPP) by a simple hydrothermal method served as an ideal SPR sensitizer for detecting trace disease markers. A 2D MOF based on Cu-TCPP was used to improve direct SPR analysis of programmed death ligand-1 exosomes (PD-L1) in human serum samples. The prepared MOF was deposited onto a gold substrate by drop casting and modified with special peptides with the ability to capture PD-L1 exosomes (Figure 22). MOF Cu-TCPP with high charge mobility contributed to the distribution of the electron concentration on the surface of the gold slide, enhancing the generation of surface plasmons and thereby increasing the sensitivity of the sensor.

It was shown that the SPR signal of the gold chip modified with 2D MOF was noticeably higher than the signal of the bare gold chip (Figure 23a). The same concentration of PD-L1 exosomes caused a change in the SPR angle when using a 2D MOF-based SPR sensor, while a pure gold-based SPR sensor caused almost no change in the SPR angle (Figure 23b). The authors explained this by using a different type of protein binding to the sensing layer. Non-specific binding of peptides occurs on the gold substrate, which

leads to disorderly attachment of peptides at the sensitive interface [107]. At the same time, in 2D MOF, porphyrin molecules can participate in the π-π interaction [108], significantly improving the binding of peptides to the sensitive interface, which facilitates the capture of target molecules and leads to an increase in the sensitivity of the SPR sensor. The LOD of the sensor based on 2D MOF Cu-TCPP was 16.7 particles/mL, and its recovery rate was 93.43–102.35%.

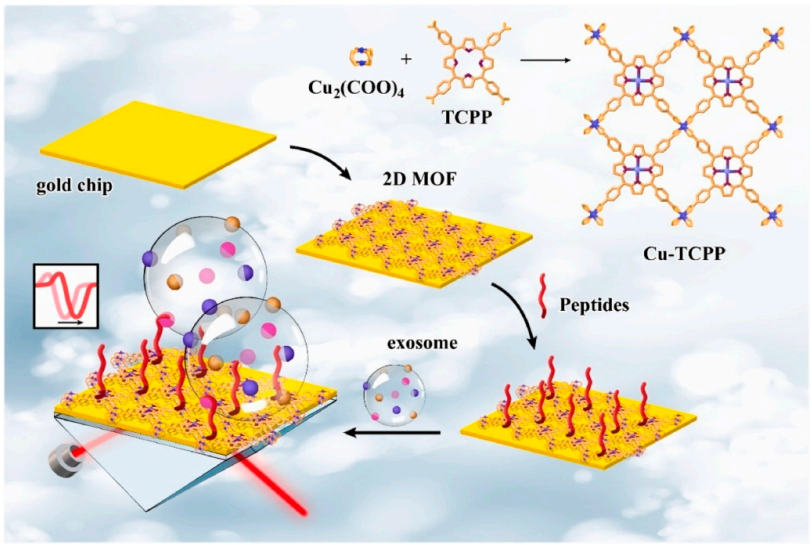

Figure 22. Schematic diagram of a 2D MOF-based SPR biosensor for simple and ultra-sensitive detection of PD-L1 exosomes. Reprinted with permission from [106]. Copyright 2022 Elsevier.

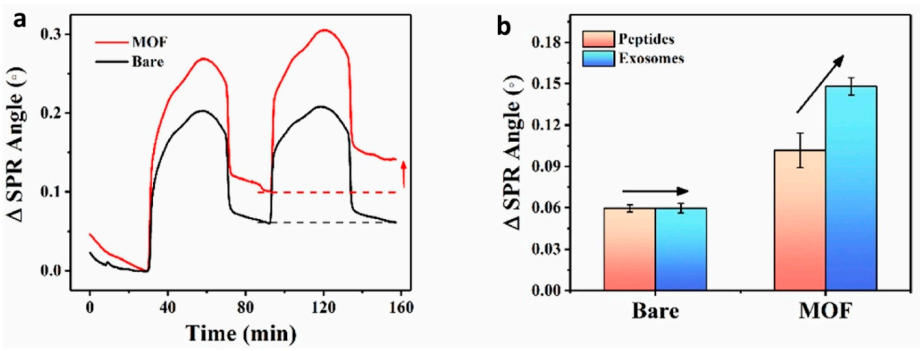

Figure 23. SPR raw signal (**a**) and data analysis (**b**) of peptides and exosomes flowed through the bare gold chip and 2D MOF chip, respectively. Reprinted with permission from [106]. Copyright 2022 Elsevier.

Later, the same group of authors [109] tested 2D MOF Cu-TCPP for the SPR detection of the antibiotic sulfamethazine (4-amino-N-(4,6-dimethyl-2-pyrimidinyl). They prepared a bilayer sensing platform based on 2D MOF Cu-TCPP, which enhances SPR, and *Para*-Sulfonatocalix [4]arene (pSC4), which provides the "specific" host–guest interaction with sulfamethazine. The prepared sensor had a LOD of only 75.54 pM and could accurately detect sulfamethazine in environmental water samples with complete recovery in the range of 95% to 110%.

Li et al. [110] also used Cu-TCPP 2D MOF to prepare an optical SPR sensor for glucose detection. The MOF was deposited onto a specially prepared arrayed resonant cavity silver film (ARC/Ag) with strong hotspots, effectively extending the sensing region (Figure 24). Due to the synergetic effect of the ordered MOF with ARC/Ag, a local electric field enhancement was observed. Glucose oxidase (GOD) was immobilized on the MOF layer by immersing the structure in the buffer solution.

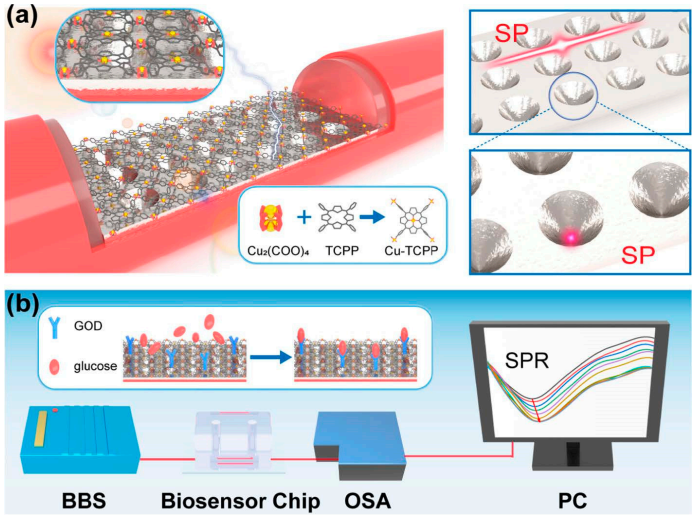

Figure 24. Schematic diagram of (**a**) the ARC/Ag/MOF sensor structure and the optical detection path (**b**). Reprinted with permission from [110]. Copyright 2023 Elsevier.

Figure 25a–c show a scheme of the reaction between glucose and GOD-ARC/Ag/MOF and a change in the position of the resonance wavelength when different concentrations of D-glucose solution (0–1.8 mg/mL) are added. The resulting sensor demonstrated high stability and a linear response factor of 9.99 nm/(mg/mL) in the range of glucose concentrations from 0.1 to 1.2 mg/mL (Figure 25d,f). The response of the sensor to glucose was noticeably higher than to ascorbic acid and uric acid (Figure 25e).

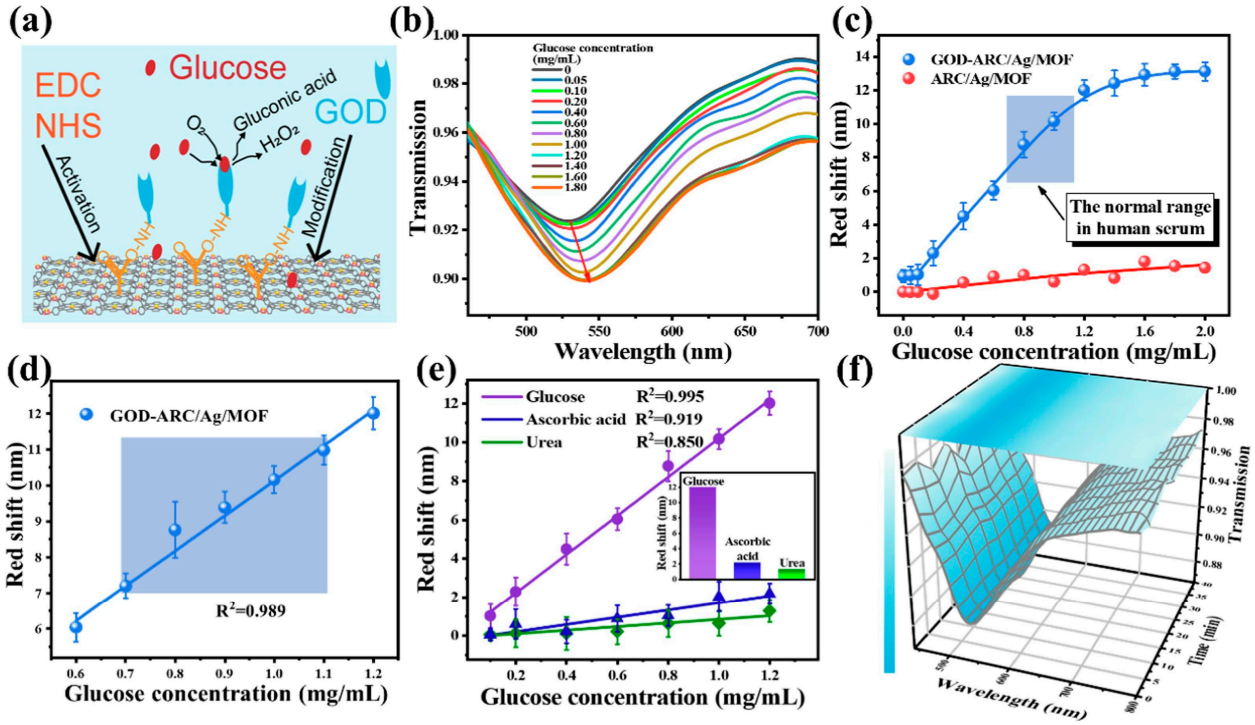

Figure 25. (**a**) Schematic diagram of the reaction between glucose and the GOD-ARC/Ag/MOF. (**b**) Normalized transmission spectra for different concentrations of glucose (0–1.8 mg/mL). (**c**) The redshift of GOD-functionalized and non-GOD-functionalized optical fibers changes with glucose concentration. (**d**) Redshift linear response of GOD-ARC/Ag/MOF at a glucose concentration of 0.6–1.2 mg/mL. (**e**) Fitting curves of selectivity for the ARC/Ag/MOF sensor. (**f**) Stability test of the GOD-ARC/Ag/MOF sensor. Reprinted with permission from [110]. Copyright 2023 Elsevier.

Kutenina et al. [111] fabricated uniformly structured surface-attached metal-organic frameworks (SURMOFs) from Zn-TCPP and zinc acetate, which were obtained as films on the surface of self-organizing monolayers of silanes and thiols by the method of layer-by-layer self-assembly. The prepared SURMOF films were utilized as sensing layers to study the qualitative SPR response to organic molecules in water solutions. It was shown that SURMOF films did not bind 4-nitrophenol and uracil, whereas they bound purine compounds, viz. adenine and adenosine 5-monophosphate. It was found by spectral methods that this binding occurred through the interaction of amino groups with Zn ions in metal clusters rather than with central metal ions in porphyrin cores.

It is known that metal nanoparticles loaded on the surface of a gold film improve the SPR signal due to the resonance coupling effect [112]. Mao et al. [113] recently used this effect to create a biosensor based on 2D MOF Cu-TCPP for the determination of Programmed Death-Ligand 1 (PD-L1), which plays an important role in regulating immune response. 2D MOF Cu-TCPP, due to its expanded conjugate surface, provides a substrate for the directional fixation of nucleic acid nanostructures through noncovalent interaction [114]. In this work, the DNA tetrahedron nanostructure was immobilized to improve the selectivity of PD-L1 detection. The sensitivity of the prepared chip was 253.31°/RIU.

Feng et al. [115] also used a structure of 2D MOF Cu-TCPP modified with gold nanoparticles (AuNPs) for the fabrication of a D-shaped fiber SPR sensor for dopamine detection. As already noted, Cu-TCPP has high electron mobility, which helps to increase the concentration of electrons on the metal surface and enhances the generation of surface plasmons. The authors showed that the Fermi level of the gold film and Cu-TCPP are close, while the value of the LUMO level of gold exceeds the value of Cu-TCPP. Under the influence of white light, electrons inside the metal are excited and move from HOMO to LUMO levels, which leads to aggregation. Due to differences in energy levels, the electrons move to the LUMO level of Cu-TCPP. The same electronic transition occurs between AuNPs and Cu-TCPP. This double electronic transition leads to an increase in the mobility of electrons inside the composite structure, thereby improving the values of the electric field on the surface of the sensing film and providing larger changes in the refractive index of the sensing layer. To improve the selectivity of dopamine detection, DNA molecules, which form hydrogen bonds with the –OH and –NH2 groups of dopamine molecules, were immobilized on the surface of a 2D Cu-TCPP MOF. The prepared AuNPs/2D MOF/Au composite structure had the linear range of the dependence of the response on the dopamine concentration from 5×10^{-14} M to 5×10^{-7} M in both PBS solution and serum samples (Figure 26) with an LOD of $1.07 \pm 0.07 \times 10^{-14}$ M. The sensor exhibited good selectivity for dopamine because the SPR response to 5×10^{-9} M of dopamine was higher than the response to interfering ascorbic (AA) and uric (UA) acids at their concentration in a solution of 5×10^{-3} M (Figure 26d). The higher sensor response was due to the specific interaction between the aptamer DNA and dopamine molecules.

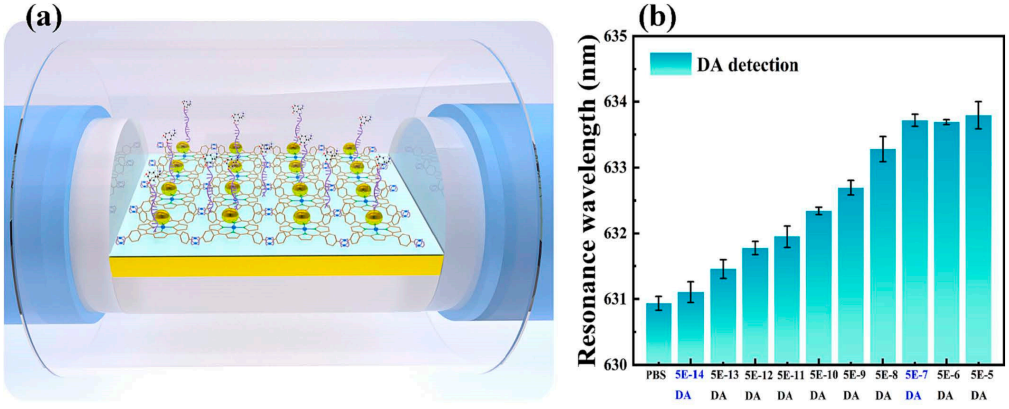

Figure 26. *Cont.*

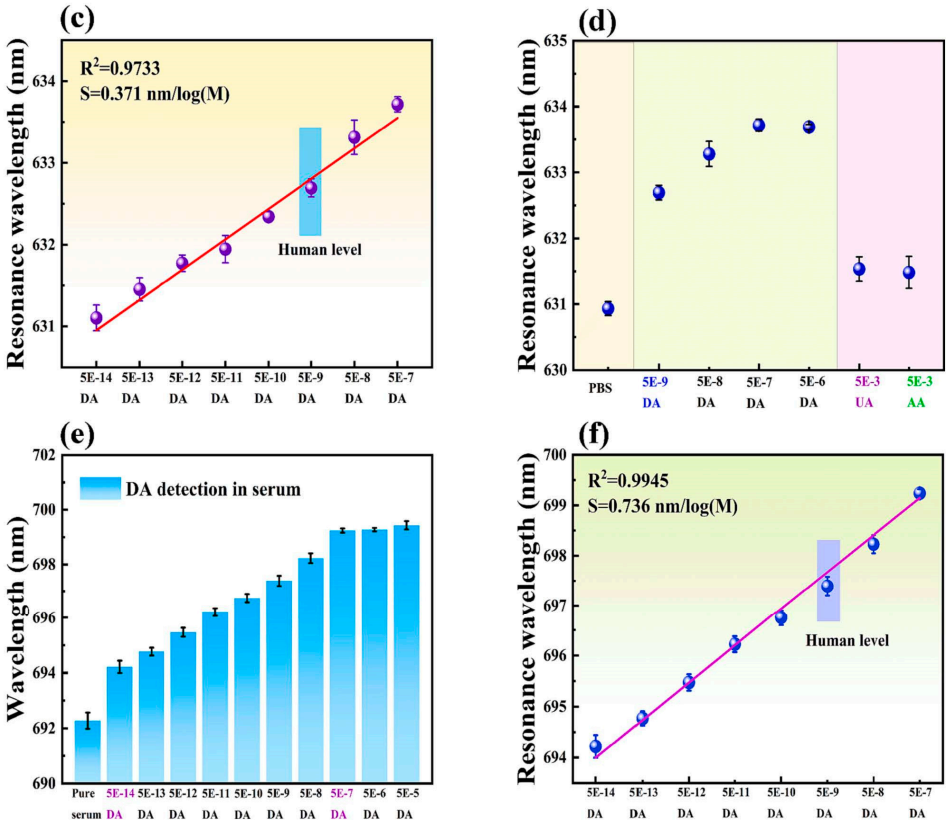

Figure 26. (**a**) The schematic diagram of dopamine (DA) solution detection by a microfluidic device. (**b**) Resonance wavelength change of DA solution with different concentrations. (**c**) The linear relationship between DA concentrations and the sensor resonance wavelength. (**d**) Comparison of the sensor response to DA (5×10^{-9} M), ascorbic acid (AA, 5×10^{-3} M), and uric acid (UA, 5×10^{-3} M) under the same experimental conditions. (**e**) Resonance wavelength change of DA in serum solution with different concentrations. (**f**) The linear relationship between the serum DA concentration and the resonant wavelength of the sensor. Reprinted with permission from [115]. Copyright 2024 Elsevier.

6. Current Issues and Future Scope

This review provided an overview of the state of research over the past fifteen years in the field of the application of porphyrins, phthalocyanines, and their hybrid materials as active layers of sensors based on the phenomenon of surface plasmon resonance. These sensors, which include classical SPR sensors and their advanced modifications such as total internal reflection ellipsometry and magneto-optical SPR techniques, are widely used for the qualitative and quantitative determination of not only gaseous analytes but also low concentrations of pesticides, herbicides, biomolecules, and even bacteria in water solutions and biological liquids.

The quantitative characteristics of some sensors for the detection of analytes in the gaseous phase and solutions are summarized in Table 6. It can be seen that SPR sensors based on phthalocyanine and porphyrin films are mainly used to detect vapors of volatile organic compounds, such as chlorinated hydrocarbons, acetic acid, and amines. The detection limit of these compounds for most sensors is units or tens of ppm, which is lower than for electrical and gravimetric sensors based on films of similar phthalocyanines and porphyrins [10,116,117]. At the same time, the response and regeneration times are only a few seconds, which is better than in their case. It should also be noted that the selectivity of SPR sensors is not very high and is comparable to the selectivity of electrical and QCM sensors.

Table 6. Examples of phthalocyanine- and porphyrin-based sensors for the detection of gaseous analytes and analytes in solutions.

Sensors for Gaseous Analytes						
Active Layer	**Method**	**Analyte**	**Sensitivity, ppm^{-1}**	**LOD, ppm**	**Response/ Recovery Time, s**	**Ref.**
CoPc, PVD film	SPR	NO_2	-	0.07	-	[41]
FCrPc, spun film	SPR	Acetic acid	57.1×10^{-7}	0.85		[43]
ZnPc5, LB film, 20 layers	SPR	Chloroform	7.97×10^{-4}	3.76	3/6	[47]
Por2, LS film, 10 layers	SPR	Acetic acid	9.82×10^{-7}	6.11		[51]
		Methylamine	4.38×10^{-7}	13.71		
ZnPP (Figure 10), LS film, 3 layers	SPR	Dibutylamine	4.32×10^{-5}	760	3/6	[55]
	MOSPR		4.31×10^{-4}	60	3/7.5	
ZnPc3j, spun film	TIRE	Trimethylamine	-	20	-	[65]
CuPc1k, spun film	TIRE	Methylamine	1.55×10^{-4}	8	158/-	[89]
CuPc1k-CNT, spun film			3.25×10^{-4}	3.6	66/-	
Sensors for analytes in solutions						
Material	Method	Analyte	Investigated concentration range	Sensitivity	LOD	Ref.
CuPc1l	TIRE	Pentachlorophenol	0.5–25 µg/L	0.00396 $(\mu g/L)^{-1}$	690 ng/L	[92]
pyridinium porphyrin mediated calix [4]arene-functionalized AuNP composites	SPR	B-type natriuretic peptide	1–10,000 pg/mL	-	0.3 pg/mL	[94]
2D MOF Cu-TCPP	SPR	Sulfamethazine	0.278–27.83 ng/mL	-	0.02 ng/mL	[109]
2D MOF Cu-TCPP modified with GOD on ARC/Ag	Optical fiber SPR	Glucose	0.1–1.2 mg/mL	9.99 nm $(mg/mL)^{-1}$	-	[110]
AuNP/2D MOF Cu-TCPP modified with DNA	Optical fiber SPR	Dopamine	5×10^{-14}–5×10^{-7} M	0.371 nm $(logM)^{-1}$	1.07×10^{-14} M	[115]

The current scenario for the development of these sensors goes in two directions. The first direction is related to the modification of substrates for SPR and the development of new research methods based on a combination of two different techniques, e.g., MSPR and SPR combined with electrochemistry. For example, using the MSPR technique makes it possible to increase the sensitivity of ZnPP-based sensors to dibutylamine by about 10 times (Table 6) compared to the classical SPR method [55].

The second direction is related to the search for new materials with a large surface area, concentration of active centers, and specificity to the investigated analytes. Along with the use of porous hybrid materials of phthalocyanines and porphyrins with metal oxides, polymers, and carbon nanotubes, in recent years much attention has been paid to the study of metal-organic frameworks based on porphyrins and phthalocyanines for use in optical sensors. 2D MOFs have a highly ordered structure and exhibit excellent electrical conductivity, high mobility of charge carriers, and highly efficient photogenerated carriers that can enhance the electric field of excitation and the surface plasmon resonance of the sensitive interface. In addition, the 2D MOF can enhance the absorption of incident light, thereby improving the output signal. In addition, due to their lamellar structure, their own surface plasmon waves may connect to the SPR of the gold film. All these properties contribute to improving the performance of the SPR sensor. This is especially important for obtaining highly sensitive sensors for the determination of low concentrations of biomolecules in

solutions, e.g., sulfamethazine, glucose, dopamine, etc. (Table 6). The selectivity of such sensors can be achieved by modifying porous 2D MOF layers with enzymes or DNA that provide specific interactions with bioanalytes. An analysis of the literature has shown that currently the set of such 2D MOF materials is limited, and, as a rule, all SPR sensors are made on the basis of tetra(4-carboxyphenyl)porphine. Therefore, the synthesis of such materials based on other derivatives of phthalocyanines and porphyrins is of particular interest. Thus, it would be useful to focus further research in the field of searching for new materials for sensors based on the SPR phenomenon on (i) obtaining hybrid materials not only with carbon nanotubes but also with graphene, since graphene has established itself as one of the best materials for improving the performance of SPR sensors on many platforms, and (ii) preparing new 2D MOFs based on porphyrins and phthalocyanines.

Funding: This research was supported by the Ministry of Science and Higher Education of the Russian Federation, project number 121031700314-5.

Institutional Review Board Statement: Not applicable.

Informed Consent Statement: Not applicable.

Data Availability Statement: Data are contained within the article.

Conflicts of Interest: The authors declare no conflicts of interest.

References

1. Mukherjee, D.; Manjunatha, R.; Sampath, S.; Ray, A.K. Phthalocyanines as Sensitive Materials for Chemical Sensors. In *Materials for Chemical Sensing*; Paixão, T.R.L.C., Reddy, S.M., Eds.; Springer: Cham, Switzerland, 2017; pp. 165–226.
2. De, S.; Devic, T.; Fateeva, A. Porphyrin and phthalocyanine-based metal organic frameworks beyond metal-carboxylates. *Dalton Trans.* **2021**, *50*, 1166–1188. [CrossRef] [PubMed]
3. Zhang, X.; Wasson, M.C.; Shayan, M.; Berdichevsky, E.K.; Ricardo-Noordberg, J.; Singh, Z.; Papazyan, E.K.; Castro, A.J.; Marino, P.; Ajoyan, Z.; et al. A historical perspective on porphyrin-based metal–organic frameworks and their applications. *Coord. Chem. Rev.* **2021**, *429*, 213615. [CrossRef] [PubMed]
4. Ji, W.; Wang, T.-X.; Ding, X.; Lei, S.; Han, B.-H. Porphyrin- and phthalocyanine-based porous organic polymers: From synthesis to application. *Coord. Chem. Rev.* **2021**, *439*, 213875. [CrossRef]
5. Basova, T.V.; Ray, A.K. Review—Hybrid Materials Based on Phthalocyanines and Metal Nanoparticles for Chemiresistive and Electrochemical Sensors: A Mini-Review. *ECS J. Solid State Sci. Technol.* **2020**, *9*, 061001. [CrossRef]
6. Magna, G.; Mandoj, F.; Stefanelli, M.; Pomarico, G.; Monti, D.; Di Natale, C.; Paolesse, R.; Nardis, S. Recent Advances in Chemical Sensors Using Porphyrin-Carbon Nanostructure Hybrid Materials. *Nanomaterials* **2021**, *11*, 997. [CrossRef] [PubMed]
7. Öztürk, Z.Z.; Kılınç, N.; Atilla, D.; Gürek, A.G.; Ahsen, V. Recent studies chemical sensors based on phthalocyanines. *J. Porphyr. Phthalocyanines* **2009**, *13*, 1179–1187. [CrossRef]
8. Bouvet, M.; Gaudillat, P.; Suisse, J.-M. Phthalocyanine-based hybrid materials for chemosensing. *J. Porphyr. Phthalocyanines* **2013**, *17*, 913–919. [CrossRef]
9. Demir, E.; Silah, H.; Uslu, B. Phthalocyanine Modified Electrodes in Electrochemical Analysis. *Crit. Rev. Anal. Chem.* **2022**, *52*, 425–461. [CrossRef] [PubMed]
10. Klyamer, D.; Bonegardt, D.; Basova, T. Fluoro-Substituted Metal Phthalocyanines for Active Layers of Chemical Sensors. *Chemosensors* **2021**, *9*, 133. [CrossRef]
11. Kumar, A.; Meunier-Prest, R.; Bouvet, M. Organic Heterojunction Devices Based on Phthalocyanines: A New Approach to Gas Chemosensing. *Sensors* **2020**, *20*, 4700. [CrossRef]
12. Klyamer, D.; Shutilov, R.; Basova, T. Recent Advances in Phthalocyanine and Porphyrin-Based Materials as Active Layers for Nitric Oxide Chemical Sensors. *Sensors* **2022**, *22*, 895. [CrossRef]
13. Paolesse, R.; Nardis, S.; Monti, D.; Stefanelli, M.; Di Natale, C. Porphyrinoids for Chemical Sensor Applications. *Chem. Rev.* **2017**, *117*, 2517–2583. [CrossRef] [PubMed]
14. Celiesiute, R.; Ramanaviciene, A.; Gicevicius, M.; Ramanavicius, A. Electrochromic Sensors Based on Conducting Polymers, Metal Oxides, and Coordination Complexes. *Crit. Rev. Anal. Chem.* **2018**, *49*, 195–208. [CrossRef]
15. Gounden, D.; Nombona, N.; van Zyl, W.E. Recent advances in phthalocyanines for chemical sensor, non-linear optics (NLO) and energy storage applications. *Coord. Chem. Rev.* **2020**, *420*, 213359. [CrossRef]
16. Francis, S.; Joy, F.; Jayaraj, H.; Sunny, N.; Rajith, L. Recent advances in porphyrin-based optical sensing. *J. Iran. Chem. Soc.* **2024**, *21*, 13–70. [CrossRef]
17. Liu, Q.; Sun, Q.; Shen, J.; Li, H.; Zhang, Y.; Chen, W.; Yu, S.; Li, X.; Chen, Y. Emerging tetrapyrrole porous organic polymers for chemosensing applications. *Coord. Chem. Rev.* **2023**, *482*, 215078. [CrossRef]

18. Simpson, T.R.E.; Cook, M.J.; Petty, M.C.; Thorpe, S.C.; Russell, D.A. Surface plasmon resonance of self-assembled phthalocyanine monolayers: Possibilities for optical gas sensing. *Analyst* **1996**, *121*, 1501–1505. [CrossRef]
19. Homola, J.; Yee, S.S.; Gauglitz, G. Surface plasmon resonance sensors: Review. *Sens. Actuators B Chem.* **1999**, *54*, 3–15. [CrossRef]
20. Shinbo, K.; Lertvachirapaiboon, C.; Ohdaira, Y.; Baba, A.; Kato, K. In-situ and simultaneous evaluation of optical absorption and deposition for phthalocyanine layer-by-layer thin films using an optical waveguide sensor utilizing surface plasmon resonance. *Jpn. J. Appl. Phys.* **2020**, *59*, 116501. [CrossRef]
21. Manera, M.G.; Ferreiro-Vila, E.; Cebollada, A.; García-Martín, J.M.; García-Martín, A.; Giancane, G.; Valli, L.; Rella, R. Ethane-Bridged Zn Porphyrins Dimers in Langmuir−Schäfer Thin Films: Spectroscopic, Morphologic, and Magneto-Optical Surface Plasmon Resonance Characterization. *J. Phys. Chem. C* **2012**, *116*, 10734–10742. [CrossRef]
22. Al Rubaye, A.; Nabok, A.; Catanante, G.; Marty, J.-L.; Takacs, E.; Szekacs, A. Detection of ochratoxin A in aptamer assay using total internal reflection ellipsometry. *Sens. Actuators B Chem.* **2018**, *263*, 248–251. [CrossRef]
23. Pant, U.; Mohapatra, S.; Moirangthem, R.S. Total internal reflection ellipsometry based SPR sensor for studying biomolecular interaction. *Mater. Today Proc.* **2020**, *28*, 254–257. [CrossRef]
24. Arwin, H. TIRE and SPR-Enhanced SE for Adsorption Processes. In *Ellipsometry of Functional Organic Surfaces and Films*; Hinrichs, K., Eichhorn, K.-J., Eds.; Springer: Berlin/Heidelberg, Germany, 2014; pp. 249–264. [CrossRef]
25. Nguyen, H.H.; Park, J.; Kang, S.; Kim, M. Surface Plasmon Resonance: A Versatile Technique for Biosensor Applications. *Sensors* **2015**, *15*, 10481–10510. [CrossRef] [PubMed]
26. Wang, Y.; Zhang, C.; Zhang, Y.; Fang, H.; Min, C.; Zhu, S.; Yuan, X.C. Investigation of phase SPR biosensor for efficient targeted drug screening with high sensitivity and stability. *Sens. Actuators B Chem.* **2015**, *209*, 313–322. [CrossRef]
27. Kretschmann, E.; Raether, H. Radiative Decay of Non Radiative Surface Plasmons Excited by Light. *Z. Naturfors A* **1968**, *23*, 2135–2136. [CrossRef]
28. Shinbo, K.; Mizusawa, K.; Takahashi, H.; Ohdaira, Y.; Baba, A.; Kato, K.; Kaneko, F.; Miyadera, N. Vapor Sensing Using Waveguide-Based Multiple Surface Plasmon Resonance Sensors. *Jpn. J. Appl. Phys.* **2011**, *50*, 01BC15. [CrossRef]
29. Shinbo, K.; Ishikawa, H.; Baba, A.; Ohdaira, Y.; Kato, K.; Kaneko, F. Fabrication of a Quartz-Crystal-Microbalance/Surface-Plasmon-Resonance Hybrid Sensor and Its Use for Detection of Polymer Thin-Film Deposition and Evaluation of Moisture Sorption Phenomena. *Appl. Phys. Express.* **2012**, *5*, 036603. [CrossRef]
30. Pockrand, I. Surface plasma oscillations at silver surfaces with thin transparent and absorbing coatings. *Surf. Sci.* **1978**, *72*, 577–588. [CrossRef]
31. Xie, Y.; Sengupta, M.; Habte, A.; Andreas, A. The "Fresnel Equations" for diffuse radiation on inclined photovoltaic surfaces (FEDIS). *Renew. Sustain. Energy Rev.* **2022**, *161*, 112362. [CrossRef]
32. Evyapan, M.; Dunbar, A.D.F. Controlling surface adsorption to enhance the selectivity of porphyrin based gas sensors. *Appl. Surf. Sci.* **2016**, *362*, 191–201. [CrossRef]
33. Kazak, A.V.; Marchenkova, M.A.; Khorkov, K.S.; Kochuev, D.A.; Rogachev, A.V.; Kholodkov, I.V.; Usol'tseva, N.V.; Savelyev, M.S.; Tolbin, A.Y. Ultrathin Langmuir–Schaefer films of slipped-cofacial J-type phthalocyanine dimer: Supramolecular organization, UV/Vis/NIR study and nonlinear absorbance of femtosecond laser radiation. *Appl. Surf. Sci.* **2021**, *545*, 148993. [CrossRef]
34. Mansur, H.S.; de Sales, N.F.; Mansur, A.A.P. Preparation and characterization of 5,10,15,20-tetraphenylporphyrin Langmuir films for gas chemsensor applications. *Surf. Interface Anal.* **2011**, *43*, 1423–1429. [CrossRef]
35. Cranston, R.R.; Lessard, B.H. Metal phthalocyanines: Thin-film formation, microstructure, and physical properties. *RSC Adv.* **2021**, *11*, 21716–21737. [CrossRef] [PubMed]
36. Klyamer, D.D.; Basova, T.V. Effect of the structural features of metal phthalocyanine films on their electrophysical properties. *J. Struct. Chem.* **2022**, *63*, 997–1018. [CrossRef]
37. Basova, T.V.; Mikhaleva, N.S.; Hassan, A.K.; Kiselev, V.G. Thin Films of Fluorinated 3d-Metal Phthalocyanines as Chemical Sensors of Ammonia: An Optical Spectroscopy Study. *Sens. Actuators B Chem.* **2016**, *227*, 634–642. [CrossRef]
38. Spadavecchia, J.; Ciccarella, G.; Rella, R. Optical characterization and analysis of the gas/surface adsorption phenomena on phthalocyanines thin films for gas sensing application. *Sens. Actuators B Chem.* **2005**, *106*, 212–220. [CrossRef]
39. Lucarini, V.; Saarinen, J.J.; Peiponen, K.-E.; Vartiainen, E.M. *Kramers–Kronigrelations in Optical Materials Research*; Springer Series in Optical Sciences; Springer: Berlin/Heidelberg, Germany, 2010; Volume 110, p. 110.
40. Opilski, Z.; Pustelny, T.; Ignac-Nowicka, J. Spectral studies of nickel-phthalocyanines. *Photon. Lett. Pol.* **2019**, *11*, 53–55. [CrossRef]
41. El-Basaty, A.B.; El-Brolossy, T.A.; Abdalla, S.; Negm, S.; Abdella, R.A.; Talaat, H. Surface plasmon sensor for NO_2 gas. *Surf. Interface Anal.* **2008**, *40*, 1623–1626. [CrossRef]
42. El-Bosaty, A.B.; El-Brolossy, T.A.; Abdalla, S.; Negm, S.; Abdella, R.A.; Talaat, H. Surface plasmon-cobalt phthalocyanine sensor for NO_2 gas. *Egypt. J. Solids* **2006**, *29*, 121–129.
43. Evyapan, M.; Kadem, B.; Basova, T.V.; Yushina, I.V.; Hassan, A.K. Study of the sensor response of spun metal phthalocyanine films to volatile organic vapors using surface plasmon resonance. *Sensors Actuators B Chem.* **2016**, *236*, 605–613. [CrossRef]
44. Basova, T.; Tsargorodskaya, A.; Nabok, A.; Hassan, A.K.; Gürek, A.G.; Gümüş, G.; Ahsen, V. Investigation of gas-sensing properties of copper phthalocyanine films. *Mater. Sci. Eng. C* **2009**, *29*, 814–818. [CrossRef]
45. Çapan, I.; Ilhan, B. Gas sensing properties of mixed stearic acid/phthalocyanine LB thin films investigated using QCM and SPR. *J. Optoelectron. Adv. Mater.* **2015**, *17*, 456–461.

46. Acikbas, Y.; Erdogan, M.; Capan, R.; Ozkaya, C.; Baygu, Y.; Kabay, N.; Gok, Y. Preparation of Zinc (II) phthalocyanine-based LB thin film: Experimental characterization, the determination of some optical properties and the investigation of the optical sensing ability. *Optik* **2021**, *245*, 167661. [CrossRef]
47. Çapan, I.; Çapan, R.; Acikbas, Y.; Baygu, Y.; Kabay, N.; Gök, Y. Chloroform sensing properties of Langmuir-Blodgett thin films of Zn(II)phthalocyanine containing 26-membered tetraoxadithia macrocycle groups. *Optik* **2023**, *294*, 171429. [CrossRef]
48. Acikbas, Y.; Erdogan, M.; Çapan, R.; Erdogan, C.O.; Baygu, Y.; Kabay, N.; Gök, Y.; Kucukyildiz, G. Preparation and characterization of the phthalocyanine–zinc(II) complex-based nanothin films: Optical and gas-sensing properties. *Appl. Nanosci.* **2023**, *13*, 4527–4540. [CrossRef]
49. Basova, T.; Kol'tsov, E.; Ray, A.K.; Hassan, A.K.; Gürek, A.G.; Ahsen, V. Liquid crystalline phthalocyanine spun films for organic vapour sensing. *Sens. Actuators B Chem.* **2006**, *113*, 127–134. [CrossRef]
50. Duran, E.N.; Çapan, I. Macrocycle ring and peripheral group sizes-dependent vapor sensing property of copper phthalocyanine thin films. *Surf. Rev. Lett.* **2020**, *11*, 2050006. [CrossRef]
51. Evyapan, M.; Hassan, A.K.; Dunbar, A.D.F. Understanding the Gas Adsorption Kinetics of Langmuir-Schaefer Porphyrin Films Using Two Comparative Sensing Systems. *Sens. Actuators B Chem.* **2018**, *254*, 669–680. [CrossRef]
52. Çapan, İ.; Özkaya, C. Characterization of Octaethyl Porphyrin Thin Films with Application to Determination of Volatile Organic Compounds. *Anal. Lett.* **2016**, *49*, 423–432. [CrossRef]
53. Çapan, İ.; Erdoğan, M.; Güner, B.; İlhan, B.; Stanciu, S.G.; Hristu, R.; Stanciu, G.A. Gas Sensing Properties of Porphyrin Thin Films Influenced by Their Surface Morphologies. *Sens. Lett.* **2014**, *12*, 1218–1227. [CrossRef]
54. Çapan, R. Porphyrin Langmuir-Blodgett Thin Film for Organic Vapor Detection, *J. Phys. Sci. Appl.* **2019**, *9*, 15–24. [CrossRef]
55. Manera, M.G.; Ferreiro-Vila, E.; García-Martín, J.M.; Cebollada, A.; García-Martín, A.; Giancane, G.; Valli, L.; Rella, R. Enhanced magneto-optical SPR platform for amine sensing based on Zn porphyrin dimmers. *Sens. Actuators B Chem.* **2013**, *182*, 232–238. [CrossRef]
56. Manera, M.G.; Rella, R. Improved gas sensing performances in SPR sensors by transducers activation. *Sens. Actuators B Chem.* **2013**, *179*, 175–186. [CrossRef]
57. Gonzalez-Diaz, J.B.; García-Martín, A.; Armelles, G.; García-Martín, J.M.; Clavero, C.; Cebollada, A.; Lucaszew, R.A.; Skuza, J.R.; Kumah, D.P.; Clarke, R. Surface-magnetoplasmon nonreciprocity effects in noble-metal/ferromagnetic heterostructures. *Phys. Rev. B.* **2007**, *76*, 153402. [CrossRef]
58. Manera, M.G.; Giancane, G.; Bettini, S.; Valli, L.; Borovkov, V.; Colombelli, A.; Lospinoso, D.; Rella, R. MagnetoPlasmonicWaves/HOMO-LUMO Free π-Electron Transitions Coupling in Organic Macrocycles and Their Effect in Sensing Applications. *Chemosensors* **2021**, *9*, 272. [CrossRef]
59. Colombelli, A.; Manera, M.G.; Borovkov, V.; Giancane, G.; Valli, L.; Rella, R. Enhanced sensing properties of cobalt bis-porphyrin derivative thin films by a magneto-plasmonic-opto-chemical sensor. *Sens. Actuators B Chem.* **2017**, *246*, 1039–1048. [CrossRef]
60. Bettini, S.; Pagano, R.; Borovkov, V.; Giancane, G.; Valli, L. The role of the central metal ion of ethane-bridged bis-porphyrins in histidine sensing. *J. Colloid Interface Sci.* **2019**, *533*, 762–770. [CrossRef] [PubMed]
61. Arwin, H.; Poksinski, M.; Johansen, K. Total Internal Reflection Ellipsometry: Principles and Applications. *Appl. Opt.* **2004**, *43*, 3028–3036. Available online: https://opg.optica.org/ao/abstract.cfm?URI=ao-43-15-3028 (accessed on 3 March 2024). [CrossRef]
62. Poksinski, M.; Arwin, H. Protein monolayers monitored by internal reflection ellipsometry. *Thin Solid Films* **2004**, *455–456*, 716–721. [CrossRef]
63. Nabok, A.; Al-Rubayea, A.G.; Al-Jawdah, A.M.; Tsargorodska, A.; Marty, J.-L.; Catanante, G.; Szekacs, A.; Takacs, E. [INVITED] Novel optical biosensing technologies for detection of mycotoxins. *Opt. Laser Technol.* **2019**, *109*, 212–221. [CrossRef]
64. Tietze, M.L.; Obst, M.; Arnauts, G.; Wauteraerts, N.; Rodríguez-Hermida, S.; Ameloot, R. Parts-per-Million Detection of Volatile Organic Compounds via Surface Plasmon Polaritons and Nanometer-Thick Metal–Organic Framework Films. *ACS Appl. Nano Mater.* **2022**, *5*, 5006–5016. [CrossRef]
65. Basova, T.V.; Hassan, A.; Krasnov, P.O.; Gürol, I.; Ahsen, V. Trimethylamine Sorption into Thin Layers of Fluoroalkyloxy and Alkyloxy Substituted Phthalocyanines: Optical Detection and DFT Calculations. *Sens. Actuators B Chem.* **2015**, *216*, 204–211. [CrossRef]
66. Yu, H.; Chong, Y.; Zhang, P.; Ma, J.; Li, D. A D-shaped fiber SPR sensor with a composite nanostructure of MoS_2-graphene for glucose detection. *Talanta* **2020**, *219*, 121324. [CrossRef] [PubMed]
67. Zheng, W.; Han, B.; Siyu, E.; Sun, Y.; Li, X.; Cai, Y.; Zhang, Y. Highly-sensitive and reflective glucose sensor based on optical fiber surface plasmon resonance. *Microchem. J.* **2020**, *157*, 105010. [CrossRef]
68. Pagano, R.; Syrgiannis, Z.; Bettini, S.; Ingrosso, C.; Valli, L.; Giancane, G.; Prato, M. Localized and surface plasmons coupling for ultrasensitive dopamine detection by means of SPR-based perylene bisimide/Au nanostructures thin film. *Adv. Mater. Interfaces* **2021**, *8*, 2101023. [CrossRef]
69. Türkmen, D.; Bakhshpour, M.; Gokturk, I.; Asir, S.; Yilmaz, F.; Denizli, A. Selective dopamine detection by SPR sensor signal amplification using gold nanoparticles. *New J. Chem.* **2021**, *45*, 18296–18306. [CrossRef]
70. Giancane, G.; Borovkov, V.; Inoue, Y.; Valli, L. Conformational switching inbis(zinc porphyrin) Langmuir-Schaefer film as an effective tool for selectively sensing aromatic amines. *J. Colloid Interface Sci.* **2012**, *385*, 282–284. [CrossRef] [PubMed]
71. Giancane, G.; Borovkov, V.; Inoue, Y.; Conoci, S.; Valli, L. Syn-anti conformation switching of a bis-porphyrin derivative at the air-water interface and in thesolid state as an effective tool for chemical sensing. *Soft Matter* **2013**, *9*, 2302–2307. [CrossRef]

72. Buccolieri, A.; Manno, D.; Serra, A.; Santino, A.; Hasan, M.; Borovkov, V.; Giancane, G. Highly sensitive conformational switching of ethane-bridged mono-zinc bis-porphyrin as an application tool for rapid monitoring of aqueous ammonia and acetone. *Sens. Actuators B Chem.* **2018**, *257*, 685–691. [CrossRef]
73. Bettini, S.; Maglie, E.; Pagano, R.; Borovkov, V.; Inoue, Y.; Valli, L.; Giancane, G. Conformational switching of ethano-bridged Cu,H_2-bis-porphyrin induced by aromatic amines. *Beilstein J. Nanotechnol.* **2015**, *6*, 2154–2160. [CrossRef]
74. Chen, T.; Xin, J.; Chang, S.J.; Chen, C.-J.; Liu, J.-T. Surface Plasmon Resonance (SPR) Combined Technology: A Powerful Tool for Investigating Interface Phenomena. *Adv. Mater. Interfaces* **2023**, *10*, 2202202. [CrossRef]
75. Ribeiro, J.A.; Sales, M.G.F.; Pereira, C. Electrochemistry combined-surface plasmon resonance biosensors: A review. *TrAC Trends Anal. Chem.* **2022**, *157*, 116766. [CrossRef]
76. Munoz, R.A.A.; Toma, S.H.; Toma, H.E.; Araki, K.; Angnes, L. Investigation of interfacial processes at tetraruthenated zinc porphyrin films using electrochemical surface plasmon resonance and electrochemical quartz crystal microbalance. *Electrochim. Acta* **2009**, *54*, 2971–2976. [CrossRef]
77. Zhou, B.; Zhang, Z.; Zhang, Y.; Li, R.; Xiao, Q.; Liu, Y.; Li, Z. Binding of Cationic Porphyrin to Human Serum Albumin Studied Using Comprehensive Spectroscopic Methods. *J. Pharm. Sci.* **2009**, *98*, 105–113. [CrossRef] [PubMed]
78. Naue, J.A.; Toma, S.H.; Bonacin, J.A.; Araki, K.; Toma, H.E. Probing the binding of tetraplatinum(pyridyl)porphyrin complexes to DNA by means of surface plasmon resonance. *J. Inorg. Biochem.* **2009**, *103*, 182–189. [CrossRef] [PubMed]
79. Perenon, M.; Bonnet, H.; Lavergne, T.; Dejeu, J.; Defrancq, E. Surface plasmon resonance study of the interaction of N-methyl mesoporphyrin IX with G-quadruplex DNA. *Phys. Chem. Chem. Phys.* **2020**, *22*, 4158–4164. [CrossRef]
80. Zangenehzadeh, S.; Agocs, E.; Jivani, H.; Könemund, L.; Neumann, L.; Hirschberg, F.; Herdan, S.; Biedendieck, R.; Jahn, D.; Roth, B.W.; et al. Bacteria detection in a Kretschmann geometry flow cell at a plasmon-enhanced interface with spectroscopic ellipsometer. *Thin Solid Films* **2023**, *764*, 139583. [CrossRef]
81. Basova, T.V.; Polyakov, M.S. Hybrid materials based on carbon nanotubes and polyaromatic molecules: Methods of functionalization and sensor properties. *Macroheterocycles.* **2020**, *30*, 91–112. [CrossRef]
82. Sisman, O.; Kilinc, N.; Akkus, U.O.; Sama, J.; Romano-Rodriguez, A.; Atilla, D.; Gürek, A.G.; Ahsen, V.; Berber, S.; Ozturk, Z. Hybrid liquid crystalline zinc phthalocyanine@Cu_2O nanowires for NO_2 sensor application. *Sens. Actuators B Chem.* **2021**, *345*, 130431. [CrossRef]
83. Coppedè, N.; Villani, M.; Mosca, R.; Iannotta, S.; Zappettin, A.; Calestani, D. Low Temperature Sensing Properties of a Nano Hybrid Material Based on ZnO Nanotetrapods and Titanyl Phthalocyanine. *Sensors* **2013**, *13*, 3445–3453. [CrossRef]
84. Sinha, M.; Verma, P.; Panda, S. Metal-phthalocyanine modified doped polyaniline for VOC sensing applications. *Flex. Print. Electron.* **2020**, *5*, 014014. [CrossRef]
85. de Barros, M.R.; Winiarski, J.P.; de Matos Morawski, F.; Marim, R.G.; Chaves, E.S.; Blacha-Grzechnik, A.; Jost, C.L. A high-performance electrochemical sensor based on a mesoporous silica/titania material and cobalt(II) phthalocyanine for sensitive pentachlorophenol determination. *Microchim. Acta* **2022**, *189*, 269. [CrossRef] [PubMed]
86. Ndebele, N.; Nyokong, T. The use of carbon-based nanomaterials conjugated to cobalt phthalocyanine complex in the electrochemical detection of nitrite. *Diam. Relat. Mater.* **2023**, *132*, 109672. [CrossRef]
87. Su, H.C.; Tran, T.-T.; Bosze, W.; Myung, N.V. Chemiresistive sensor arrays for detection of air pollutants based on carbon nanotubes functionalized with porphyrin and phthalocyanine derivatives. *Sens. Actuators Rep.* **2020**, *2*, 100011. [CrossRef]
88. Sharma, A.K.; Debnath, A.K.; Aswal, D.K.; Mahajan, A. Room temperature ppb level detection of chlorine using peripherally alkoxy substituted phthalocyanine/SWCNTs based chemiresistive sensors. *Sens. Actuators B Chem.* **2022**, *350*, 130870. [CrossRef]
89. Banimuslem, H.; Hassan, A.; Basova, T.; Esenpınar, A.A.; Tuncel, S.; Durmuş, M.; Gürek, A.G.; Ahsen, V. Dye-modified carbon nanotubes for the optical detection of amines vapours. *Sens. Actuators B Chem.* **2015**, *207*, 224–234. [CrossRef]
90. Banimuslem, H.; Hassan, A.; Basova, T.; Durmuş, M.; Tuncel, S.; Esenpınar, A.A.; Gürek, A.G.; Ahsen, V. Copper phthalocyanine functionalized single-walled carbon nanotubes: Thin films for optical detection. *J. Nanosci. Nanotechnol.* **2015**, *15*, 2157–2167. [CrossRef] [PubMed]
91. Banimuslem, H.; Hassan, A.; Basova, T.; Yushina, I.; Durmuş, M.; Tuncel, S.; Esenpınar, A.A.; Gürek, A.G.; Ahsen, V. Copper Phthalocyanine Functionalized Single-Walled Carbon Nanotubes: Thin Film Deposition and Sensing Properties. *Key Eng. Mater.* **2014**, *605*, 461–464. [CrossRef]
92. Hassan, A.; Banimuslem, H.; Basova, T.; Gülmez, A.D.; Durmus, M.; Gürek, A.G.; Ahsen, V. Surface interaction of copper phthalocyanine modified single walled carbon nanotubes with pesticides. *Sens. Actuators B Chem.* **2016**, *224*, 780–788. [CrossRef]
93. Banimuslem, H.; Hassan, A.; Basova, T.; Gülmez, A.D.; Tuncel, S.; Durmuş, M.; Gürek, A.G.; Ahsen, V. Copper phthalocyanine/single walled carbon nanotubes hybrid thin films for pentachlorophenol detection. *Sens. Actuators B Chem.* **2014**, *190*, 990–998. [CrossRef]
94. Zhu, Z.; Li, H.; Xiang, Y.; Koh, K.; Hu, X.; Chen, H. Pyridinium porphyrins and AuNPs mediated bionetworks as SPR signal amplification tags for the ultrasensitive assay of brain natriuretic peptide. *Microchim. Acta* **2020**, *187*, 327. [CrossRef] [PubMed]
95. Lv, Y.-Y.; Xu, W.; Lin, F.-W.; Wu, J.; Xu, Z.-K. Electrospun nanofibers of porphyrinated polyimide for the ultra-sensitive detection of trace TNT. *Sens. Actuators B Chem.* **2013**, *184*, 205–211. [CrossRef]
96. Lv, Y.-Y.; Wu, J.; Wan, L.-S.; Xu, Z.-K. Novel Porphyrinated Polyimide Nanofibers by Electrospinning, *J. Phys. Chem. C* **2008**, *112*, 10609–10615. [CrossRef]

97. Rella, R.; Rizzo, A.; Licciulli, A.; Siciliano, P.; Troisi, L.; Valli, L. Tests in controlled atmosphere on new optical gas sensing layers based on TiO_2/metal-phthalocyanines hybrid system. *Mater. Sci. Eng. C* **2002**, *22*, 439–443. [CrossRef]
98. Berrier, A.; Offermans, P.; Cools, R.; van Megen, B.; Knoben, W.; Vecchi, G.; Rivas, J.G.; Crego-Calama, M.; Brongersma, S.H. Enhancing the gas sensitivity of surface plasmon resonance with a nanoporous silica matrix. *Sens. Actuators B Chem.* **2011**, *160*, 181–188. [CrossRef]
99. Olorunyomi, J.F.; Geh, S.T.; Caruso, R.A.; Doherty, C.M. Metal–organic frameworks for chemical sensing devices. *Mater. Horiz.* **2021**, *8*, 2387–2419. [CrossRef] [PubMed]
100. Shen, Y.; Tissot, A.; Serre, C. Recent progress on MOF-based optical sensors for VOC sensing. *Chem. Sci.* **2022**, *13*, 13978–14007. [CrossRef] [PubMed]
101. Philip, A.; Kumar, A.R. Two-dimensional materials and their role in sensitivity enhancement of surface plasmon resonance based biosensor. *Trends Anal. Chem.* **2024**, *171*, 117497. [CrossRef]
102. Kreno, L.E.; Hupp, J.T.; Van Duyne, R.P. Metal-Organic Framework Thin Film for Enhanced Localized Surface Plasmon Resonance Gas Sensing. *Anal. Chem.* **2010**, *82*, 8042–8046. [CrossRef]
103. Koh, C.S.L.; Sim, H.Y.F.; Leong, S.X.; Boong, S.K.; Chong, C.; Ling, X.Y. Plasmonic Nanoparticle-Metal-Organic Framework (NP-MOF) Nanohybrid Platforms for Emerging Plasmonic Applications. *ACS Mater. Lett.* **2021**, *3*, 557–573. [CrossRef]
104. Vandezande, W.; Janssen, K.P.F.; Delport, F.; Ameloot, R.; De Vos, D.E.; Lammertyn, J.; Roeffaers, M.B.J. Parts per Million Detection of Alcohol Vapors via Metal Organic Framework Functionalized Surface Plasmon Resonance Sensors. *Anal. Chem.* **2017**, *89*, 4480–4487. [CrossRef] [PubMed]
105. Yuan, Y.; Peng, X.; Weng, X.; He, J.; Liao, C.; Wang, Y.; Liu, L.; Zeng, S.; Song, J.; Qu, J. Two-dimensional nanomaterials as enhanced surface plasmon resonance sensing platforms: Design perspectives and illustrative applications. *Biosens. Bioelectron.* **2023**, *241*, 115672. [CrossRef] [PubMed]
106. Wang, Y.; Mao, Z.; Chen, Q.; Koh, K.; Hu, X.; Chen, H. Rapid and sensitive detection of PD-L1 exosomes using Cu-TCPP 2D MOF as a SPR sensitizer. *Biosens. Bioelectron.* **2022**, *201*, 113954. [CrossRef] [PubMed]
107. Guo, Y.; Tao, J.; Li, Y.; Feng, Y.; Ju, H.; Wang, Z.; Ding, L. Quantitative localized analysis reveals distinct exosomal protein-specific glycosignatures: Implications in cancer cell subtyping, exosome biogenesis, and function. *J. Am. Chem. Soc.* **2020**, *142*, 7404–7412. [CrossRef] [PubMed]
108. Huang, C.-F.; Yao, G.-H.; Liang, R.-P.; Qiu, J.-D. Graphene oxide and dextran capped gold nanoparticles based surface plasmon resonance sensor for sensitive detection of concanavalin A. *Biosens. Bioelectron.* **2013**, *50*, 305–310. [CrossRef] [PubMed]
109. Wang, Y.; Niu, Z.; Xu, C.; Zhan, M.; Koh, K.; Niu, J.; Chen, H. 2D MOF-enhanced SPR sensing platform: Facile and ultrasensitive detection of Sulfamethazine via supramolecular probe. *J. Hazard. Mater.* **2023**, *456*, 131642. [CrossRef]
110. Li, Y.; Liu, W.; Liu, R.; Gao, J.; Feng, J.; Xu, S.; Li, Z.; Jiang, S.; Du, X. 3D hybrid arrayed Ag/MOF multi-plasmon resonant cavity system for high-performance SPR sensing. *Optics Laser Technol.* **2023**, *167*, 109825. [CrossRef]
111. Kutenina, A.P.; Zvyagina, A.I.; Raitman, O.A.; Enakieva, Y.Y.; Kalinina, M.A. Layer-by-Layer Assembly of SAM-Supported Porphyrin-Based Metal Organic Frameworks for Molecular Recognition. *Colloid J.* **2019**, *81*, 401–410. [CrossRef]
112. Zhang, Y.-J.; Chen, S.; Radjenovic, P.; Bodappa, N.; Zhang, H.; Yang, Z.-L.; Tian, Z.-Q.; Li, J.-F. Probing the Location of 3D Hot Spots in Gold Nanoparticle Films Using Surface-Enhanced Raman Spectroscopy. *Anal. Chem.* **2019**, *91*, 5316–5322. [CrossRef]
113. Mao, Z.; Zheng, W.; Hu, S.; Peng, X.; Luo, Y.; Lee, J.; Chen, H. Multifunctional DNA scaffold mediated gap plasmon resonance: Application to sensitive PD-L1 sensor. *Biosens. Bioelectron.* **2024**, *247*, 115938. [CrossRef]
114. Hu, P.-P.; Liu, N.; Wu, K.-Y.; Zhai, L.-Y.; Xie, B.-P.; Sun, B.; Duan, W.-J.; Zhang, W.-H.; Chen, J.-X. Successive and Specific Detection of Hg^{2+} and I^- by a DNA@MOF Biosensor: Experimental and Simulation Studies. *Inorg. Chem.* **2018**, *57*, 8382–8389. [CrossRef] [PubMed]
115. Feng, J.; Li, Y.; Jiang, M.; Jiang, S.; Gao, J.; Yang, W.; Liu, R. A reliable gold nanoparticle/Cu-TCPP 2D MOF/gold/D-shaped fiber sensor based on SPR and LSPR coupling for dopamine detection. *Appl. Surf. Sci.* **2024**, *655*, 159523. [CrossRef]
116. Harbeck, M.; Erbahar, D.D.; Gürol, I.; Musluoglũ, E.; Ahsen, V.; Öztürk, Z.Z. Phthalocyanines as sensitive coatings for QCM sensors operating in liquids for the detection of organic compounds. *Sens. Actuators B. Chem.* **2010**, *150*, 346–354. [CrossRef]
117. Baygu, Y.; Çapan, R.; Erdogan, M.; Ozkaya, C.; Acikbas, Y.; Kabay, N.; Gok, Y. Synthesis, characterization and chemical sensor properties of a novel Zn(II) phthalocyanine containing 15-membered dioxa-dithia macrocycle moiety. *Synth. Met.* **2021**, *280*, 116870. [CrossRef]